UNIVERSIDADE D
COIMBRA

Rafaela Lourenço Graça Antunes

APPLICATION OF ADDITIVE MANUFACTURING POLYMERS IN FRAMEWORKS OF FULL-ARCH IMPLANT-SUPPORTED FIXED PROSTHESES

Thesis submitted to the Faculty of Sciences and Technology of the University of Coimbra for the degree of Master in Biomedical Engineering with specialization in Biomaterials, supervised by Prof. Dra. Maria Augusta Neto and Prof. Dra. Ana Lúcia de Pereira Neves Messias.

2021

1 2  9 0

FACULDADE DE CIÊNCIAS E TECNOLOGIA
UNIVERSIDADE D COIMBRA

Rafaela Lourenço Graça Antunes

Application of additive manufacturing polymers in frameworks of full-arch implant-supported fixed prostheses

Dissertation to obtain the Master's Degree in Biomedical Engineering, with specialization in Biomaterials

Supervisors:
Prof. Dra. Maria Augusta Neto (DEM)
Prof. Dra. Ana Lúcia de Pereira Neves Messias (FMUC)

Coimbra, 2021

This work was developed in collaboration with:

CEMMPRE - Center for Mechanical Engineering, Materials and Processes

FMUC - Faculdade de Medicina da Universidade de Coimbra

Agradecimentos

Não posso deixar de agradecer a todas as pessoas que me ajudaram neste percurso e sem as quais a conclusão deste projeto não seria possível.

Em primeiro lugar, gostaria de deixar um agradecimento especial às minhas orientadoras. À Prof. Dra. Augusta Neto, pelo conhecimento transmitido na área da biomecânica e dos elementos finitos, pela constante disponibilidade e ajuda na resolução de problemas. À Prof. Dra. Ana Messias, por me introduzir no mundo da medicina dentária, por me acompanhar e incentivar a descobrir esta área. Obrigada por me acolherem no vosso grupo de trabalho e por me guiarem quando estava fora da minha zona de conforto. Estou-vos muito grata pelo companheirismo, pelo tempo gasto comigo no laboratório e pela boa disposição mesmo depois de várias horas de trabalho. Tudo isto tornou o caminho mais fácil.

Quero agradecer também à Prof. Dra. Ana Amaro, que desde sempre se disponibilizou para me ajudar no que fosse preciso e que dava sempre uma palavra de motivação quando passava na sala Prof. Nuno Rilo.

A todos os que gastaram um pouco do seu tempo para me ajudar - o Prof. Vitor Maranha (DEM), a Prof. Dra. Ana Paula Piedade (DEM), o Nuno Cruz (ISEC), o Sr. Fernando (Oficinas do DEM) - o meu muito obrigada.

Aos meus amigos de Coimbra, obrigada por me acompanharem durante estes anos e por os tornarem inesquecíveis. Aos meus amigos de Oleiros, por me apoiarem sempre, mesmo muitas vezes estando longe. Obrigada por não me deixarem desmotivar. Levo-vos a todos para a vida!

Por fim, mas não menos importante, quero agradecer à minha família. Às minhas avós, pelo amor incondicional. À minha irmã, por ser um exemplo para mim em todos os sentidos e por ser a conselheira de todas as horas. Aos meus pais, por serem os grandes impulsionadores de tudo, por me deixarem seguir os meus sonhos e estarem sempre lá para mim.

Abstract

Edentulism, the irreversible loss of natural teeth, is considered a disability by the World Health Organization (WHO) that still affects a significant part of the population. Implant-Supported Fixed Prostheses (ISFPs) are a reliable and well-accepted type of restoration to treat edentulous jaws, conventionally made of a framework of metal or metal alloys and obtained by Subtractive Manufacturing (SM). However, these structures have a high modulus of elasticity, which increases weight and stress in the structure that can be transferred to the bone and cause discomfort to the patient. In addition, the time between diagnosis, fabrication, and implementation of restorations is still high.

With this in mind, the present study aimed to compare the behavior of frameworks made of polymeric and non-polymeric materials, but also to test two different types of techniques to fabricate them.

First, using the software ADINA®, a numerical study of a framework was performed in two 3D models upgraded to mimic the protocol application in ISFPs. These simulations allowed the comparison of the displacement and effective stress of different materials. Then, in an experimental analysis using the software VIC-3D, frameworks and complete prostheses made of polymers obtained with Additive Manufacturing (AM) and SM techniques were tested. Two AM processes were used: Fused Deposition Modeling (FDM) and Selective Laser Sintering (SLS). The displacement and the deformations were obtained.

The simulations allowed to confirm that polymeric frameworks present lower values of effective stress, highlighting the polymers PMMA and OXPEKK. However, they also display higher values of displacement. The experimental study suggested that the SLS process has a better performance when compared to the other AM technique and close to the other milled polymers. Although the experiment gave good indications, further studies are necessary.

Resumo

Edentulismo, perda irreversível de dentes naturais, é considerada uma deficiência pela Organização Mundial de Saúde (OMS) que ainda afeta uma parte significativa da população. Próteses Fixas Implanto-Suportadas (PFIS) são um tipo de restauro indicado para tratamento de arcadas dentárias totalmente edêntulas, convencionalmente composto por uma subestrutura feita de metais ou ligas metálicas obtidas por Manufatura Subtrativa (MS). No entanto, estas estruturas possuem elevado módulo de elasticidade, aumentando o peso e a tensão na estrutura que pode vir a ser transferida para o osso e causar desconforto ao paciente. Além disso, o tempo entre o diagnóstico, o fabrico e a implementação destes restauros ainda é elevado.

Com isto em mente, o presente estudo teve como objetivo comparar o comportamento de subestruturas feitas de materiais poliméricos e não-poliméricos, mas também testar dois tipos de técnicas de fabrico diferentes.

Primeiro, utilizando o software ADINA®, foi efetuado um estudo numérico de uma subestrutura em dois modelos 3D melhorados para replicar o protocolo de aplicação em PFIS. Estas simulações permitiram a comparação do deslocamento e da tensão de diferentes materiais. Depois, numa análise experimental com recurso ao software VIC-3D, subestruturas e próteses completas feitas de polímeros obtidos por técnicas de Manufatura Aditiva (MA) e MS foram testados. Dois tipos de processos de MA foram utilizados: *Fused Deposition Modeling* (FDM) e *Selective Laser Sintering* (SLS). Os deslocamentos e as deformações foram obtidas.

As simulações permitiram confirmar que subestruturas poliméricas apresentam valores menores de tensão, com destaque para os polímeros PMMA e OXPEKK. No entanto, estes polímeros apresentam também os maiores valores de deslocamento. O estudo experimental sugeriu que os materiais fabricados por SLS apresentam um comportamento mais favorável do que aqueles fabricados por FDM, e próximo do comportamento dos polímeros fresados. Apesar do estudo ter dado boas indicações, são necessários estudos mais aprofundados.

Contents

List of Figures

List of Tables

List of Abbreviations

ABS Acrylonitrile Butadiene Styrene.
ADINA Automatic Dynamic Incremental Nonlinear Analysis.
AM Additive Manufacturing.

CAD/CAM Computer-Aided Design/Computed-Aided Manufacturing.
CBCT Cone Beam Computed Tomography.
Co-Cr Cobalt-Chromium.
CT Computed Tomography.

DEMUC Departamento de Engenharia Mecânica da Universidade de Coimbra.
DIC Digital Image Correlation.

E Modulus of Elasticity.

FDM Fused Deposition Modeling.
FEM Finite Element Method.
FRC Fiber-Reinforced Composite.

HIPS High Impact Polystyrene.

ISFP Implant-Supported Fixed Prosthesis.
ISFPs Implant-Supported Fixed Prostheses.

OPM Oxford Performance Materials.

PAEK Polyaryletherketone.
PEEK Polyetheretherketone.
PEKK Polyetherketoneketone.
PET-G Polyethylene Terephthalate Glycol.
PLA Polylactic Acid.
PMMA Polymethylmetacrylate.

SLS Selective Laser Sintering.
SM Subtractive Manufacturing.

Ti Titanium.

WHO World Health Organization.

ZrO_2 Zirconia.

1

Introduction

In this chapter, there is a brief introduction of the motivation (section 1.1), the expected goals (section 1.2) and the structure of the document (section 1.3).

1.1 Motivation

Polymeric materials, due to their properties that can be wide and easily adapted, are now used in a lot of different areas. Dentistry is not an exception and over the past few years, the development of new materials along with new production technologies, broadened the options available for treatments. Computer-Aided Design/Computed-Aided Manufacturing (CAD/CAM) technologies allow the fabrication of customized structures, that can be previously planned and designed to make devices as accurate as possible, minimizing the need for changes after the final implantation and increasing the patients' comfort [23].

There is evidence that teeth loss affects general health, so patients that experience irreversible loss of teeth show decreased oral and general health. To overcome these issues and make treatments more accessible to patients, it is important to access new materials and techniques to fabricate them. The framework of Implant-Supported Fixed Prostheses (ISFPs) is normally obtained by Subtractive Manufacturing (SM), in which blocks of material are milled to become smaller structures; this leads to an excessive amount of wasted material. The use of Additive Manufacturing (AM), in which structures are built from zero, reduces not only the waste of material but also the time between diagnosis and implementation of this type of restoration since this technique produces structures in a relatively short period of time. However, in the field of prosthetic dentistry, the use of polymers and AM is still limited, due to the lack of long-term clinical reports and because the printing conditions need to be optimized [24].

The use of polymers and AM techniques, also known as 3D printing, could be a cost-effective solution in implant dentistry, with the reduction of structures' weight

and modulus of elasticity, decreasing the stress transferred to the bone and teeth. This can be also used in patients that need this type of treatment but have metal allergies. 3D printers are becoming a lot more affordable and with a variety of processes available [23, 25].

1.2 Expected goals

The main goal is to investigate the performance of polymeric frameworks of implant-supported prostheses and compare the performance with conventional non-polymeric ones obtained by SM and AM techniques. The first step is the analysis of the structures using the Finite Element Method (FEM). After this numerical validation of the frameworks, an experimental setup was created to compare polymeric frameworks and complete prosthesis obtained by the different techniques.

1.3 Structure of the document

This document contains 4 chapters beyond the introduction:

- Chapter 2 – Literature Review - presents the most relevant information related to topic, the problems associated and the state of the art.
- Chapter 3 – Methodologies - is where the experimental methods and its conditions are explained, along with the models used.
- Chapter 4 – Results and Discussion - shows the numerical and experimental results, with the respective statistical analysis and comparison between the different materials.
- Chapter 5 – Conclusion and Future Work - is the last chapter, where the conclusions of the study are presented and some suggestions for future work.

2

Literature Review

This chapter presents the concepts needed for a clear understanding of the main topic and state of the art.

2.1 Edentulism

A healthy oral cavity contains teeth in two arches: maxillary (upper) and mandibular (lower). The permanent dentition is composed of 32 teeth, divided equally into both the arches: 4 incisors, 2 canines, 4 premolars, and 6 molars (see figure 2.1) [4]. Teeth, along with the craniofacial complex, allow us to comfortably speak, smile, chew and do some other essential actions [26].

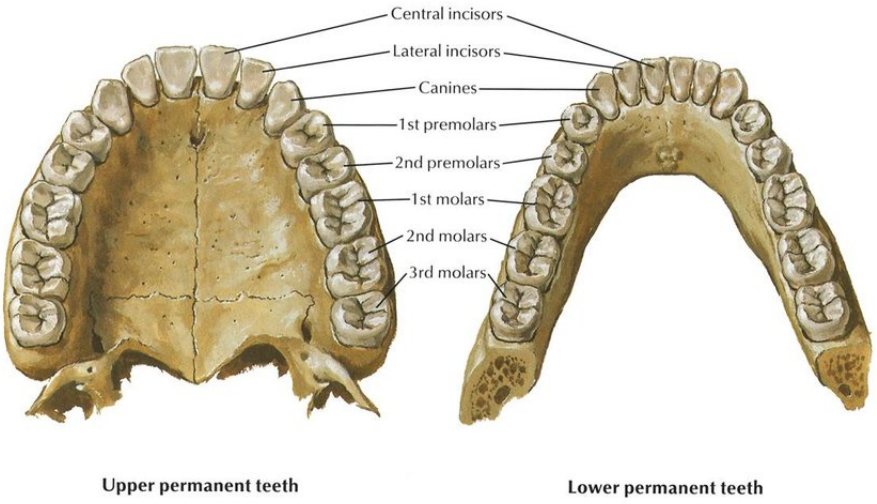

Figure 2.1: Types of permanent dentition: occlusal view of the maxilla and mandible (from left to right) [1].

Edentulism is considered a disability by the World Health Organization (WHO), characterized by an irreversible loss of natural teeth. The main causes of this condition are untreated caries and periodontal disease. The progression of the disease

is affected by several factors, such as poor dental hygiene, inability to get access to proper care, level of education, and the choice of lifestyle [27].

An edentulous patient suffers from a decrease in oral health and consequently general health. Tooth loss is followed by bone loss, as seen in figure 2.2, which leads to adverse aesthetic and biomechanical effects. Consequently, compromising chewing and eating affect nutritional intake and have a negative impact on diet and food selection. Besides the functional limitations, edentulism influences the psychological and social ability of the individuals, which shows decreased self-esteem and difficulties in socializing. Edentulous patients are more likely to also develop systemic diseases. Influencing day-to-day activities, there is a significant decrease in patients' quality of life [3, 26].

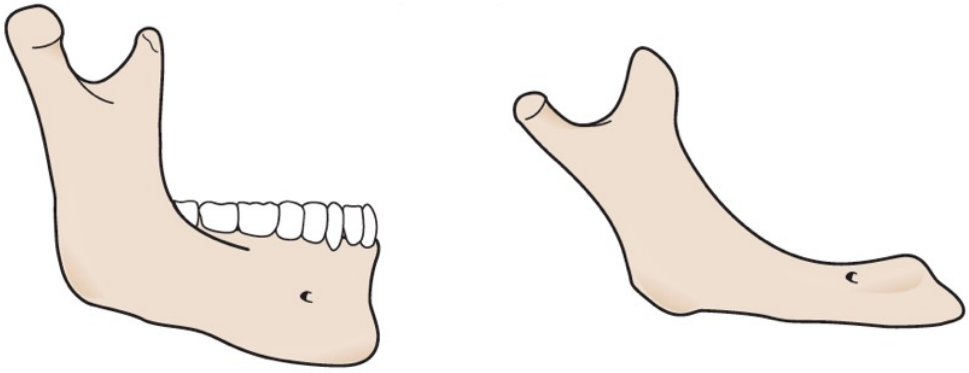

(a) **(b)**

Figure 2.2: Changes in the mandible: (a) Healthy mandible of an adult; (b) Edentulous mandible with a visible decrease of bone volume (adapted from [2]). Bone loss affects the mandible four times more than the maxilla [3].

Complete edentulism is characterized by the loss of all teeth and partial edentulism is the loss of some teeth. Although the number of completely edentulous patients is decreasing, the disease remains a major worldwide issue, especially amongst older people. Since average life expectancy is increasing, the need for this type of treatment may persist [3].

2.2 Prosthetic Rehabilitation

A prosthetic rehabilitation intends to replace lost teeth with an artificial substitute and can range from one tooth to an entire dentition (as exemplified in figure 2.3). Edentulous patients rely on prostheses for proper oral function and to restore their appearance [27, 28].

Prostheses can be classified based on different aspects:

- Mobility: removable or fixed;
- Support: implant-, teeth- or tissue-supported;
- Dimension: partial (replacing just one or a few teeth) or total/complete (restoring a dental arch or even the entire dentition) [27, 29].

Before choosing the type of restoration, a clinical evaluation of the patient and the edentulous area must be performed to check, amongst other things, if the remaining height and width of bone are viable for the procedure [4, 29].

(a) **(b)**

Figure 2.3: Examples of prostheses: (a) Partial removable prosthesis, replacing posterior teeth; (b) Single-tooth fixed implants (a lateral incisor on top, and a first molar below) [4].

Both removable and fixed prostheses are well-accepted treatments for edentulous patients. But, since each case is different, the advantages and disadvantages of the types of restoration should be carefully examined [4].

In this study, we focused on Implant-Supported Fixed Prostheses (ISFPs).

2.2.1 Implant-supported fixed prostheses

ISFPs are a type of restoration that requires the use of one or more implants placed in the residual bone to support and keep the prosthesis steady (figure 2.4). Fixed prostheses have more stability when compared to removable ones, which can be an important factor for the patient when choosing the type of prosthesis [4, 29, 30]. Messias et al. [31] concluded with a numerical study that implant-assisted removable prostheses have better support and retention when compared to conventional removable prostheses, demonstrating the importance of implants in reducing the displacement of the restoration and increasing the patient's comfort.

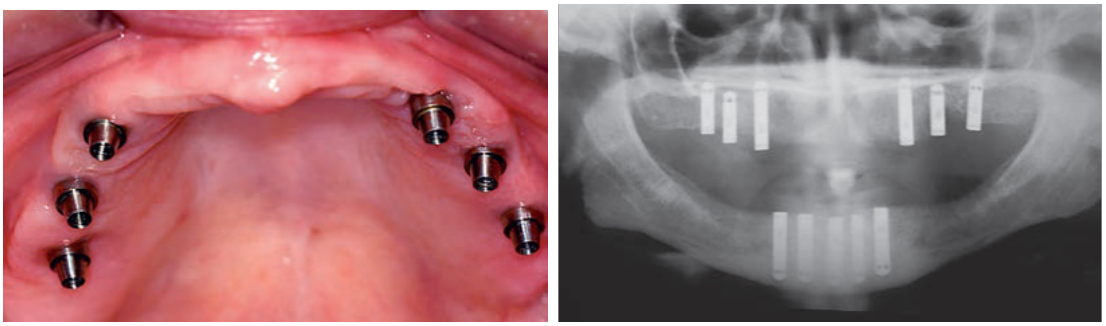

(a) **(b)**

Figure 2.4: Different views after implant placement: (a) Intraoral view of the superior implants; (b) Radiography of all the implants, inferior and superior [4].

Normally, the implants are made of metal or metal alloys (for example, titanium or Ti-6Al-4V alloy). The number and placement of the implants are determined by each specific case and by the dimension of the edentulous area [7, 30]. Figure 2.5 depicts a complete line of implant, where different variations of components are shown.

Figure 2.5: Complete line of implant: (1) Screw; (2) Link; (3) Multi-unit; (4) Implant fixture [5].

2.2.2 Full-arch implant-supported fixed prostheses

Full-arch ISFPs are a type of total prostheses made to replace completely edentulous jaws. The base of the restoration is the framework that is screwed to the implant, conventionally made of metal/metal alloys but more recently tested with fiber-reinforced composites and polymers. The framework is made to support and distribute the stress equally between the implants. To simulate teeth and gingiva, ceramic or polymeric materials are used, such as acrylic resin (see figure 2.6). These

materials that coat the framework and simulate the natural appearance of the teeth and gingiva are called veneering materials [4, 19, 30].

The use of complete dentures/prostheses that don't include the framework is a possibility. The teeth and gingiva already printed/milled would just be painted with tissue-colored resin [16].

(a) **(b)**

Figure 2.6: Example of polymeric frameworks: (a) Initial framework; (b) Frameworks with addition of some artificial teeth and gingiva [6].

Usually, the number of implants in a full-arch restoration ranges from 4 to 6; only if necessary, more implants should be used [4]. Some complications can arise, and the patient needs to be aware of the importance of maintenance in order to reduce the risks. Framework fracture, implant failure, damage of the veneering materials are some of the possible problems [30].

Since ISFPs need to be comfortable and long-lasting, the process requires a careful choice of procedure, implant position, and prosthetic material. Techniques to fabricate prostheses and new materials that reduce the cost of treatments must be analyzed, to make rehabilitation more accessible to patients [26].

2.3 Fabrication of the prostheses

Ever since the emergence of CAD/CAM, the workflow to develop a dental prosthetic rehabilitation became a fast and digital process, allowing the production of patient-specific prostheses. This process can be divided in three main steps:

- Scanning: to obtain digital images of the area to restore, several methods can be used, such as Computed Tomography (CT) for hard tissues and impression

for the soft tissues;

- Design: after obtaining a virtual image of the patient's mouth, it is possible to design a precise restoration using CAD software;
- Fabrication: two distinct methods are used to fabricate the prostheses: Subtractive Manufacturing (SM) and Additive Manufacturing (AM) [8, 32, 33].

2.3.1 Subtractive Manufacturing

Conventional prostheses are produced through SM, which refers to the fabrication of objects by removing excess from a solid block of material. This process is also known as milling and consists of a machine with a cutting tool to shape the material, controlled by the computer. Figure 2.7 shows the fabrication of a framework from a disk of material. The gold standard frameworks in prosthetic dentistry are still made by SM [7, 32].

Figure 2.7: Example of a framework being milled [7].

2.3.2 Additive Manufacturing

AM techniques are based on the fabrication of objects layer-by-layer, and they are the opposite of SM. As depicted in figure 2.8, the virtual model is divided into slices with the same thickness, then gradually printed. The layer thickness, printing angulation and orientation depend on the object to print [8, 33].

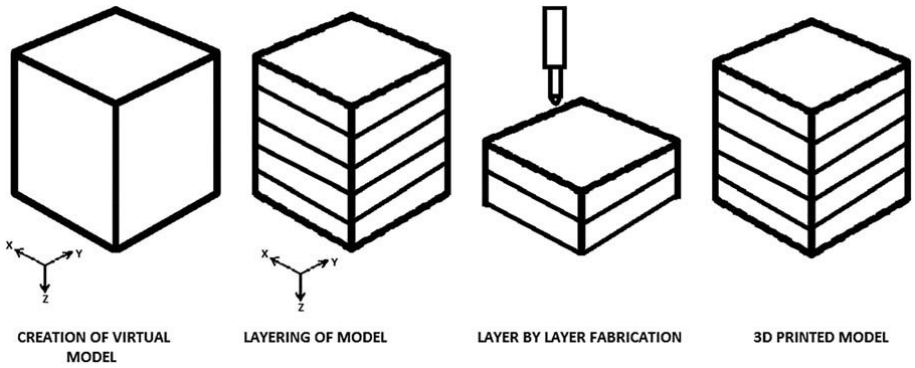

Figure 2.8: Additive manufacturing process [8].

Different printers display different attributes that influence the quality of the object obtained:

- Resolution: the smallest element that can be replicated by the printer;
- Precision: the ability to reproduce the same object with equal dimensions;
- Trueness: the capacity to print the object with the same dimensions of the design [33].

Each printer also has different post-processing procedures that can affect the final object. For this reason, samples of the same material obtained from different machines can differ [33].

The two different AM techniques used in this study are explained below.

Fused Deposition Modeling

Fused Deposition Modeling (FDM) is based on the extrusion of material from a nozzle. In this structure, which is located in the extrusion head, the material is heated before being deposited at a certain pressure. It is important to maintain the rate of deposition and the temperature of the printer, to guarantee layers' homogeneity. The nozzle can move in 3 directions, whereas the platform moves in one. Figure 2.9 shows a simplification of the process [9].

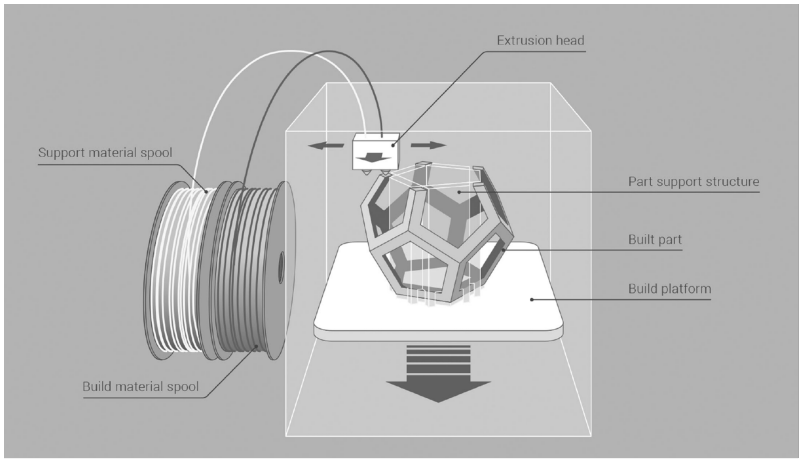

Figure 2.9: Example of FDM technology, with the different components that compose the printer [9].

Selective Laser Sintering

Selective Laser Sintering (SLS) is a powder-based AM technique that uses a laser to "selectively" sinter or fuse the material according to the CAD design. As seen in figure 2.10, a roller pushes the material to the fabrication powder bed, where the laser densifies only the particles that will form the object (getting into the brown state). The existence of a powder bed allows the construction of the desired structure without support material and without restricting the design of internal features [34]. Once the printing is complete, the object is scooped and post-processed to remove the excess of powder [21].

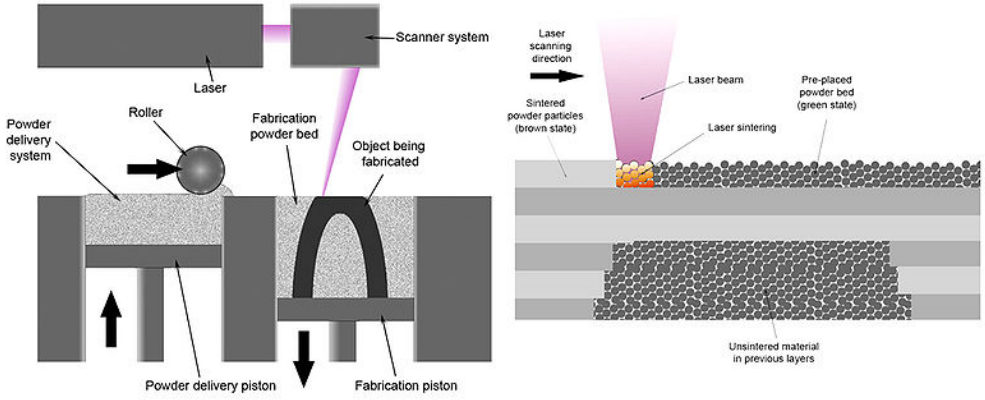

Figure 2.10: Example of SLS technique: on the left, a scheme that shows the general process; on the right, a closer look at the laser step [10].

3D printing allows the use of new materials that are constantly appearing in the market. The properties of these new addictive manufacturing polymers need to

be studied to validate (or not) their use in the field of prosthetic dentistry [35].

2.4 Materials

As referred previously, rigid frameworks have been the gold standard to treat edentulous arches. Some of these materials are metals or metal alloys such as Titanium (Ti), Cobalt-Chromium (Co-Cr), and ceramics such as Zirconia (ZrO_2). Replacing these structures with ones that have lower elastic modulus can reduce cost, weight, and stress distributed to the bone [19].

The materials used in this study are introduced in the next subsections.

2.4.1 PEEK

Polyetheretherketone (PEEK) is a synthetic polymer that enters the Polyaryletherketone (PAEK) family, a group of high-performance polymers that exhibit higher performance and properties when compared to standard ones [11]. In a report by Papathanasiou et al. [25], in vitro studies showed that PEEK has good mechanical and physical properties, chemical stability, and high biocompatibility. The in vivo studies included the use of PEEK in frameworks of ISFPs and removable partial dentures. Sirandoni et al. [19] used the Finite Element Method (FEM) to study different framework materials in Implant-Supported Fixed Prosthesis (ISFP) to replace an edentulous mandible. These studies included PEEK, which showed decreased values of stress in the framework, when compared to metal and ceramic. This can be related to the lower Young's Modulus or Modulus of Elasticity (E) of the polymer, with a value close to 4 GPa, meaning that it isn't as rigid as metal frameworks (such as titanium) and it's closer to human bone. Figure 2.11 shows the chemical structure of PEEK.

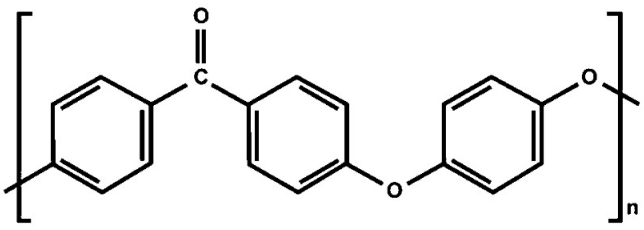

Figure 2.11: Chemical structure of the monomer unit of PEEK (adapted from [11]).

2.4.2 PEKK

Polyetherketoneketone (PEKK) is also a type of PAEK. Due to the presence of one more ketone group and with an E close to 5 GPa, this polymer shows a higher melting temperature and a more rigid structure when compared to PEEK. The problem that is common in high-performance polymers is that they are inert, which means that would be problems with adhesion [36]. Alqurashi et al. [37] compiled an overview of the use of PEKK in dentistry, that include applications in frameworks of ISFP and removable dentures. This material was also studied as a framework material with the FEM by Lee et al. [20].

2.4.3 OXPEKK

OXPEKK is an alternative formulation based on PEKK, developed by the enterprise Oxford Performance Materials (OPM). OXPEKK is the powder that is posteriorly processed by SLS. The difference between PEKK and OXPEKK is the ratio of the two monomers that can exist, depicted in figure 2.12. In OXPEKK there is a ratio of 60/40, which results in a new formulation with a decrease in the modulus of elasticity. This material was already tested in cranial implants but no reports are available on the use of this material in dentistry [21].

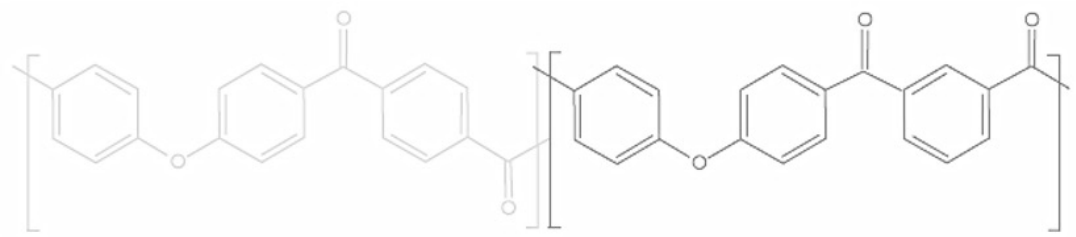

Figure 2.12: Chemical structure of the two monomers of PEKK, that have a ratio of 60/40 in OXPEKK, respectively (adapted from [12]).

2.4.4 PMMA

Polymethylmetacrylate (PMMA) is widely known as a substitute for glass, with its first use taking place in World War II, for example in airplane windows. When some of these windows shattered and accidentally cut the eyes of soldiers, the damages were much less severe than those of conventional glass, showing that it was more compatible with human tissues. Later, this and some other features were confirmed, such as good thermal and chemical stability, and also great mechanical strength [38]. The chemical structure of the monomer of PMMA is represented in

figure 2.13. In an article previously referred in subsection 2.4.1, Sirandoni et al. also tested PMMA in a framework, showing decreased values of stress, when compared to more rigid frameworks. This material was already used in ISFPs, mainly interim prostheses [39].

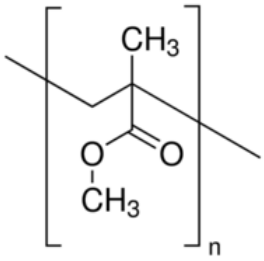

Figure 2.13: Chemical structure of the monomer of PMMA [13].

2.4.5 Trilor

Trilor is an Fiber-Reinforced Composite (FRC) formulation developed by the enterprise Bioloren® to offer a non-metal dentistry solution. These materials have biomechanical properties close to that of dentine and human bone, making them good candidates for restorations. Compared to polymers from the PAEK family, FRC have better adhesion which can result in fewer failures [6, 7]. Trilor is already accepted as a material to use in frameworks, with successful outcomes in short period follow-ups [40].

2.4.6 ABS

Acrylonitrile Butadiene Styrene (ABS) is also a thermoplastic known for its ease of processability and use in different applications. The fusion of three monomers, represented in figure 2.14, results in a combination of chemical and thermal stability, rigidity, and impact strength. It is used as a 3D printed polymer, for example in medical devices, but its application in dentistry is still minimal [14, 41].

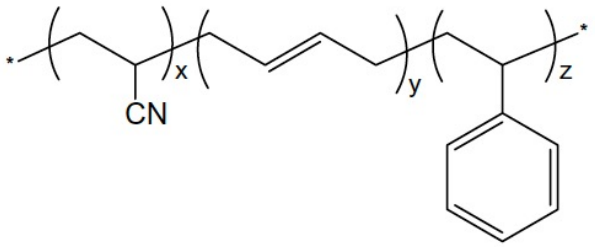

Figure 2.14: Molecular structure of ABS [14].

2.4.7 HIPS

High Impact Polystyrene (HIPS) is a development of polystyrene, composed of a continuous polystyrene phase and a small amount of disperse rubber, such as polybutadiene. This special structure brings high toughness quality with a low production cost, making HIPS a good option in our study. No reports of the use of this material in dentistry were found [42, 43]. The molecular structure of HIPS is represented in figure 2.15.

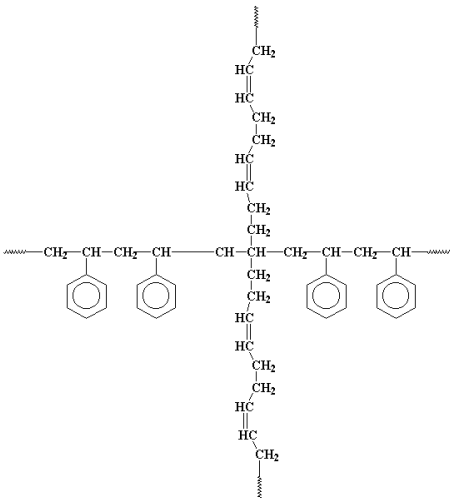

Figure 2.15: Chemical structure of HIPS [15].

2.5 State of the Art

Some of the polymers previously referred have been tested in medical areas, such as orthopedic and cranial implants (OXPEKK, PMMA), scaffolds (PMMA), synthetic membranes (ABS) and dentistry (PEEK, PEKK, Trilor) [41, 44]. Revilla-León et al. [9] gathered in an article the applications of polymers obtained with AM techniques in dentistry: surgical guides, custom trays, working casts and provisional restorations.

The next paragraphs are about some reports of frameworks or complete prostheses obtained with SM techniques, but no long-term reports are available. The main concern is the performance of the prostheses after a long period (minimum of 5 years).

Malo et al. [44] reported a short-term study to evaluate the use of a PEEK framework in a full-arch ISFP to rehabilitate edentulous jaws, where the structure was milled from a disk and a primer was applied before the veneering materials. One month after the procedure, the survival rate was of 98% in 49 prosthesis, with only

one patient in need of replacement due to fracture. Five prostheses showed problems in veneer adhesion, and 10.2% had mechanical complications. In terms of patient's comfort, 88% were comfortable using the restoration and 84% were satisfied with the performance of it when chewing.

Papathanasiou et al. [25] put together the currently available literature on the use of PEEK in dentistry. A significant number of in vitro studies were made, with some of the following outcomes: PEEK and PMMA showed decreased von Mises stresses in frameworks but with highest deformations than conventional materials; lower reinforcement of PEEK frameworks compared to FRC and cobalt-chromium-molybdenum alloy; lower failure load of PEEK when compared to ZrO_2 and nickel-chromium alloy. Three in vitro studies using PEEK frameworks showed favorable esthetics, comparable with that of ceramic restorations and cushion of occlusal loads. Also, the reduced weight and lower E can make the prosthetic more comfortable for the patient.

In another short publication, Dawson et al. [45] suggested the use of PEKK in the framework of complete and removable fixed prostheses, but with no clinical trials. Oh et al. [46] reported the use of a PEKK framework for the reconstruction of a mandible of a 70-year old after a bone graft. The one-year follow-up showed no signs of mechanical complications. Recent articles compiled the prospects for the use of PEEK and PEKK in dentistry, such as implants, crowns, bridges, removable denture components and fixed prostheses. A limited number of studies is available, so more evaluations of the materials are necessary [11, 37].

Passaretti et al. [7] proposed a protocol for the replacement of an edentulous mandible with a full-arch ISFP made of milled FRC. With the use of this material and minimally invasive surgery, the author predicts a good performance of the prosthesis combined with less cost and energy transferred to the bone. No follow-up is available.

Fewer reports of restorations made with AM techniques are available. Oh et al. [16] presented a technique to fabricate an interim ISFP in a fast and precise way, combining intraoral scanning, Cone Beam Computed Tomography (CBCT), Computer-Aided Design/Computed-Aided Manufacturing (CAD/CAM), and 3D printing. After the digital design of the surgical template and restoration, both structures are 3D printed using a printable resin (figure 2.16). Printing the teeth as part of the structure and without needing adhesive, lowers the possibility of fracture. This report showed good framework esthetic and an efficient workflow but no information about the longevity of the provisional restoration (figure 2.17).

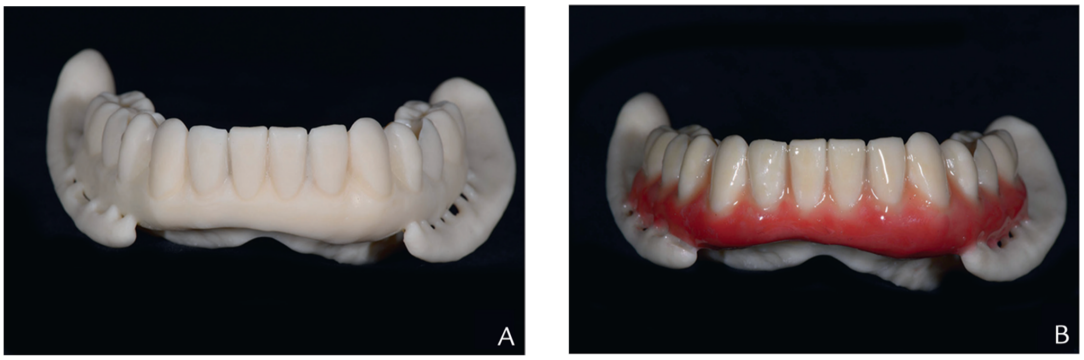

Figure 2.16: 3D printed prosthesis: (A) After printing; (B) After applying tissue-colored resin. The material not painted is used to reposition the prosthesis in the mouth, and after that, it is cut [16].

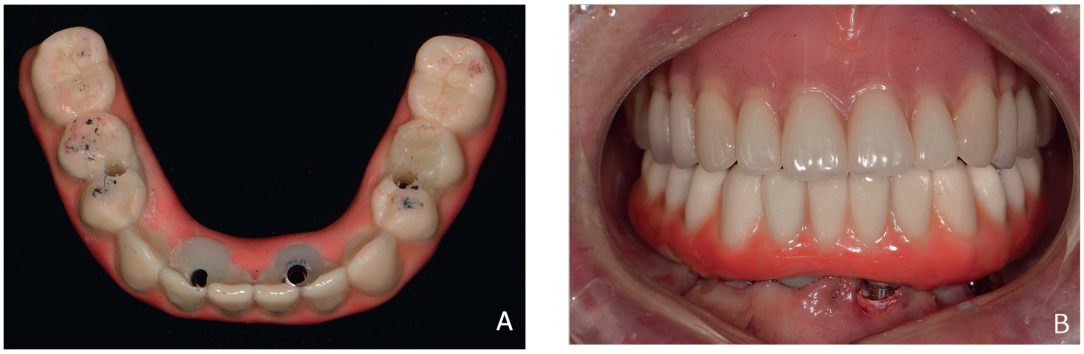

Figure 2.17: (A) Occlusal view of the prosthesis, showing the cylinders to screw the structure to the implants; (B) Facial view of the prosthesis, after positioning in the maxilla [16].

3

Methodologies

This chapter presents a basic description of the methods used to study the prosthetic components. In the numerical evaluation are explained some modifications applied in the initial 3D model of the framework and the conditions simulated. Then, two models are experimentally tested, and all the steps that preceded the tests are detailed.

3.1 Finite Element Method

The term Finite Element Method (FEM) was created in 1960 by R. W. Clough, with a lot of contributions made in the 1950s by other authors, and has become an essential tool in the analysis of major engineering and scientific problems [47]. Mechanic problems are expressed in a set of partial differential equations that are hard or even impossible to solve by analytic methods. Numeric methods cannot give exact solutions to the problems but achieve approximations [48]. Since this method allows the establishment of physical properties and the repetition of different conditions in the system, it is a non-invasive way that contrasts with experimental techniques. With the use of advanced imaging techniques, some improvements have been recently made in the replication of in vivo condition; however, the analysis with FEM needs to be complemented with in vitro studies since the complete replication of conditions is complicated [49].

FEM is used to study and simulate the biomechanical behavior of prostheses of complex geometry, namely medical devices placed inside the human body, providing initial information about the performance of the structures studied. In dentistry, this technique has been used to evaluate the patterns of displacement and stress in implant/prosthesis components but also bone and teeth [49]. For instance, in a recent paper, Messias et al. [50] described the use of the FEM to study different designs of implant-assisted removable partial dentures and to compare their performances with the performance of a conventional removable partial denture.

With this method, the user can input the known properties of materials that compose the model, the restrictions, contacts, loading and boundary conditions. The other main steps of the FEM are domain discretization, displacement approximation, and the formulation of the finite element equation [17, 48].

3.1.1 Domain Discretization

The first step of the method can be considered its basis, which is the division of a continuous structure into a certain number of finite elements, made of edges and nodes (figure 3.1). This allows the division of a complex structure into elements with simpler geometries. The shape of the finite elements and the mesh of the domain are created by connecting the nodes [17, 48].

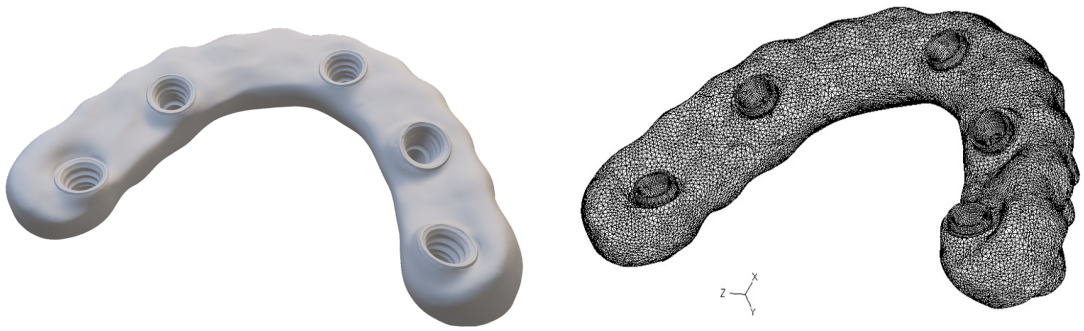

(a) **(b)**

Figure 3.1: (a) Continuous model; (b) Model with mesh.

The most common 3D elements are tetrahedrons or hexahedrons, as seen in figure 3.2 [17].

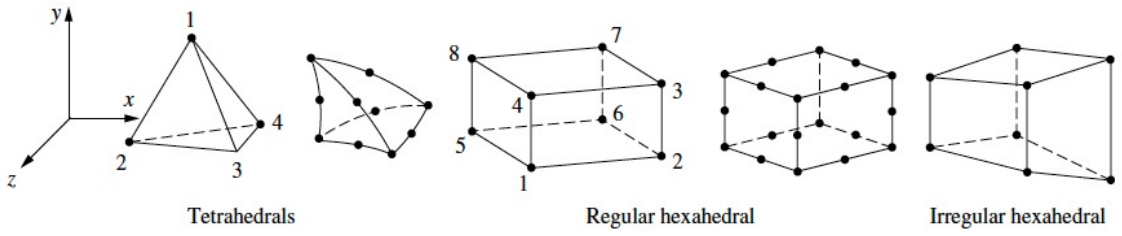

Figure 3.2: The most used 3D elements: tetrahedrons and hexahedrons [17].

The elements should be small enough to assure the correctness of the solution; however, if the elements are too small, there is a risk of overlapping and the induction of more computational costs. Mesh quality is hard to define, but it can influence

the accuracy of the simulation. For example, in areas where there is a larger stress gradient, a thinner mesh can be favorable [48].

3.1.2 Displacement Approximation

This step requires the attribution of a coordinate system to each finite element that is its reference system. The displacement can be interpolated using this reference position, taking into consideration the geometric limits at the element nodes [48]. The equation of the interpolation is

$$\tilde{u}(\bar{x}_1,\bar{x}_2,\bar{x}_3) = \bar{N}(\bar{x}_1,\bar{x}_2,\bar{x}_3)\bar{u} \tag{3.1}$$

where the $\tilde{u}$ is the approximation of displacements, $\bar{u}$ the nodal displacement, $\bar{N}$ the matrix with the interpolation functions and $\bar{x}_1$, $\bar{x}_2$, $\bar{x}_3$ the coordinates. The procedure to define shape functions is well explained in Neto et al. [48]. In general, for the approximation of displacement in each element, the number of interpolation functions or shape functions should at least equal the number of element nodes. These functions are mainly of polynomial type, which facilitates the differentiation of integration of the equations [48].

3.1.3 Finite Element Equations

The finite element equations are obtained by assembling the equations of each finite element created during the discretization phase and can be written as

$$M\ddot{U} + KU = F \tag{3.2}$$

where M is the mass matrix, K the stiffness matrix, $\ddot{U}$ the acceleration vector, U the vector of global displacements and F the vector of nodal forces. If the external forces applied are constant in time, the analysis can be considered static, which means that the acceleration vector factor ($\ddot{U}$) can disappear. The equation in this case is

$$KU = F \tag{3.3}$$

that once solved, gives the nodal degrees of freedom. With these results, displacement, stress, and strain can also be obtained [48].

3.2 3D CAD Models

Initially, a model of a framework for a mandibular full-arch Implant-Supported Fixed Prosthesis (ISFP) was used. The model is pictured in Figure 3.3 and has 62mm of length and 39mm of height. As seen, it has five holes with a diameter of 5mm to assemble the implants; the hole gains a conical shape and becomes smaller till reaching a diameter of 3.6mm. The position of these holes depends on each specific clinical case, but the goal should be to reduce the tension in each implant site and have an equal distribution in the framework.

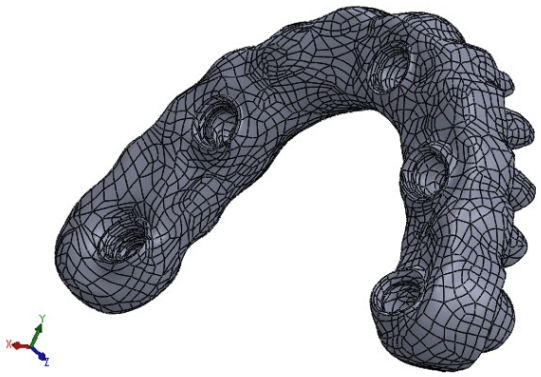

Figure 3.3: Initial model of the framework.

3.2.1 Model 1

The model of figure 3.4 was upgraded to mimic the protocol application of a framework in a full-arch ISFP. Hence, it was combined with five metallic links and the glue (cyanoacrylate) that bonds the links to the framework, using the 3D CAD software SolidWorks®. The glue has the shape of the hole, with an approximate height of 9.65mm, a maximum diameter of 5mm that decreases till reaching a minimum diameter of 3.6mm. The links fit in this set, with a maximum diameter of 5mm and an inner diameter of 2.3mm. Figure 3.4 shows the new components and the model after the assembly. To simplify, this model will be called **Model 1**. This step was made with the help of professor Vitor Maranha (DEMUC).

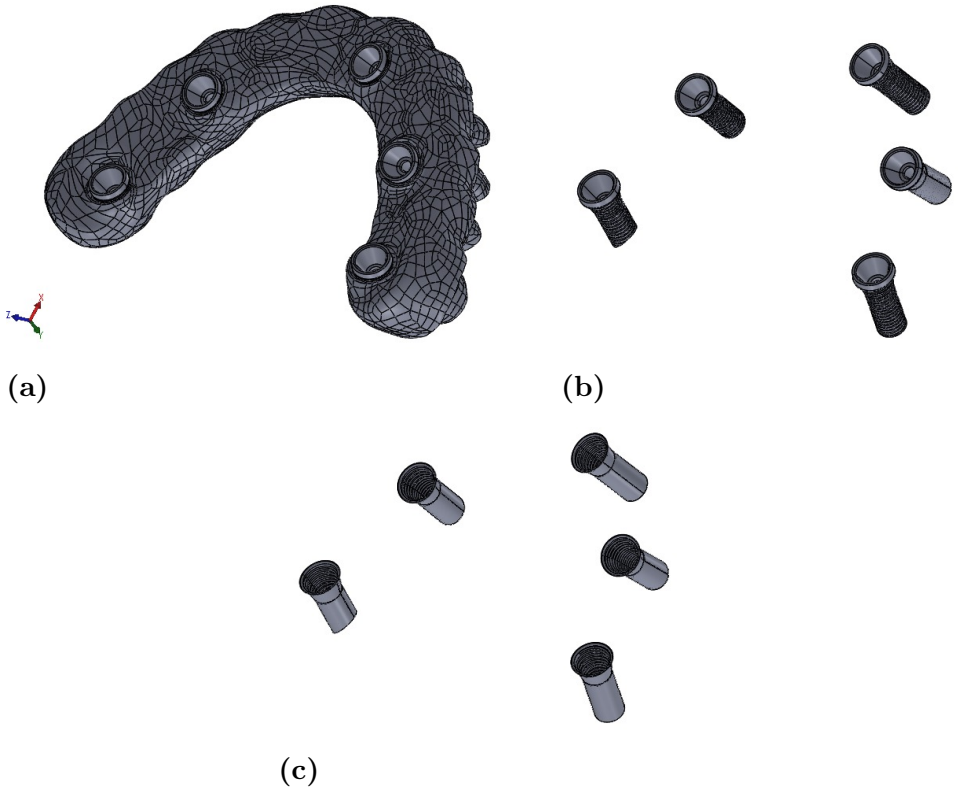

Figure 3.4: New model after the first upgrade: (a) Model 1; (b) Links; (c) Glue.

3.2.2 Model 2

After some simulations using the first model, another upgrade of the model was made also using SolidWorks®. This modification has the purpose of getting an even more realistic framework applied in a full-arch ISFP. Connected to the links, a structure was inserted to mimic the multi-units used to attach the implant. These structures have 3.5mm of height and three different outer diameters: 4.4mm, 4.8mm, and 2.3mm (from top to bottom). The top surfaces of these new components, parallel to the framework, were fixated to see if there are any dissipated tensions between the multi-units and the links. This model will be called from now on **Model 2** and is depicted in Figure 3.5.

(a) **(b)**

Figure 3.5: New model after the second upgrade: (a) Model 2; (b) Multi-units.

3.3 Numerical Analysis

There are several available FEM softwares, but the one used in this numeric study was the Automatic Dynamic Incremental Nonlinear Analysis (ADINA)® systems. After the assembly of the pieces, the model was exported to a Parasolid format (.x_t) and then imported to the ADINA® systems for the finite element analysis. In this process, the point coincidence was checked with a tolerance of $1x10^{-7}$ m.

This finite element study aimed to make an initial comparison of the mechanical behavior of different framework materials, metallic and non-metallic. Seven simulations were made in both models, one for each framework material, using the properties that are presented in table 3.1. All of the materials were considered isotropic linear elastic.

Table 3.1: Properties of the materials used in the models [6, 19–22].

Structure	Material	Young's Modulus (GPa)	Poisson's ratio
Framework	PEEK	4.1	0.4
	PEKK	5.1	0.4
	OXPEKK	3.7	0.4
	PMMA	3	0.38
	Trilor	26	0.4
	Titanium	115	0.35
	Co-Cr	218	0.33
Links	Titanium	115	0.35
Glue	Cyanoacrylate	1.33	0.4
Multi-units	Titanium	115	0.4

Contact pairs were created between all the components (table 3.2). The "tar-

get" surface is the first to be charged by the load, and just after that, the "contactor". The glue-mesh algorithm was used because the structures were considered perfectly bonded in both models, as they should be in reality after the assembly.

Table 3.2: Contact pairs and the algorithm used.

Model	Target	Contactor	Algorithm
1, 2	Framework	Glue	Glue-mesh
1, 2	Glue	Link	Glue-mesh
2	Link	Multi-unit	Glue-mesh

All bodies were divided into smaller elements based on the desired edge length, which is presented in table 3.3. With the definition of the elements, a mesh is created to simplify the complex geometry. The type of element used was the hexahedron, with 8 nodes, created with the free-form algorithm. Figures 3.6 and 3.7 show the mesh originated in Model 1 and Model 2, respectively.

Table 3.3: Length of the elements' edge.

Bodies	Model 1 (mm)	Model 2 (mm)
Framework	0.5	0.5
Links	0.2	0.2
Glue	0.2	0.2
Multi-units	-	0.3

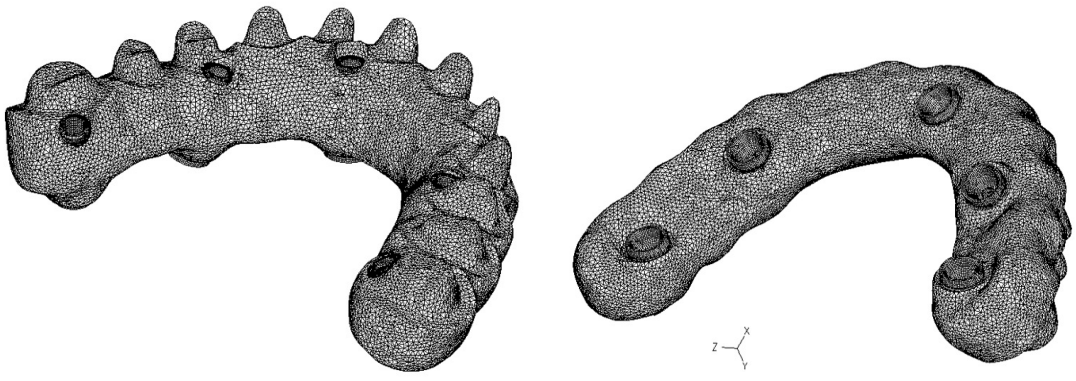

(a) **(b)**

Figure 3.6: Mesh discretization of the first framework assemblage: Model 1.

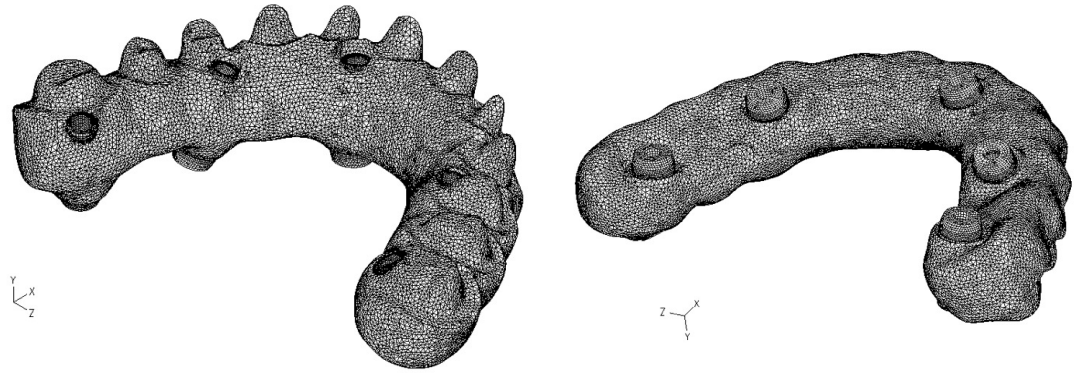

(a) **(b)**

Figure 3.7: Mesh discretization of the second framework assemblage: Model 2.

The framework was loaded by a 100N load at the surfaces where the second premolars of the model will be placed, to simulate chewing forces. On the literature, Ferreira et al. [51] simulated the occlusal forces with a load on the first molars. A lot of alternatives to simulate forces are reported, but since we use the same load in the different materials, comparison of results between them is possible [51].

The load was applied as pressure, meaning that was distributed perpendicular to the surface, as shown in figure 3.8. The total right area of application is 20.1 μm^2 and the left one 13.5 μm^2.

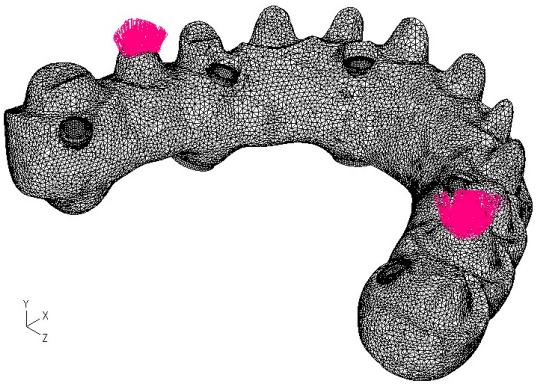

Figure 3.8: Load applied on the second premolar of both sides of the framework.

On both models, the boundary conditions were applied on the surface of the last structure added, with the three degrees of freedom fixed. On model 1 the boundary is the upper surface of the links and on model 2 the upper surface of the multi-units (see figure 3.9).

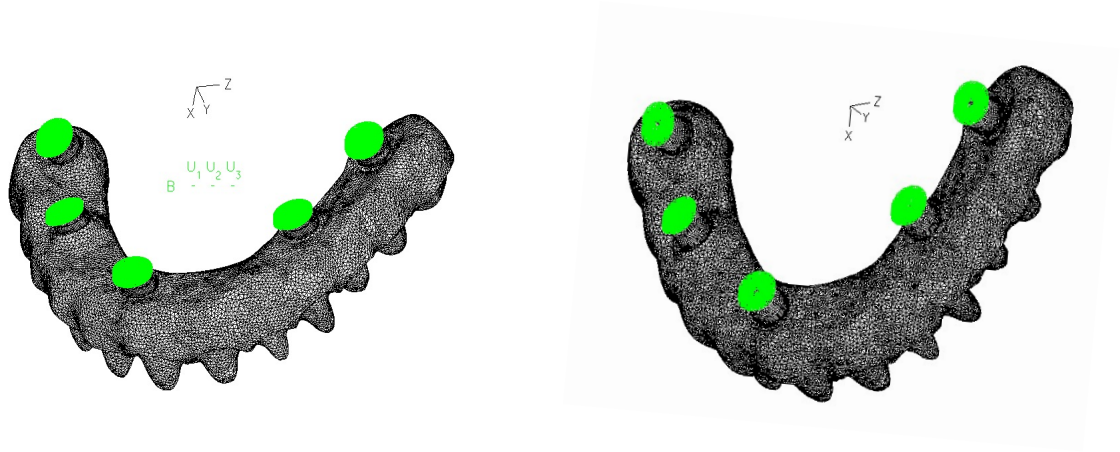

Figure 3.9: Boundary conditions of Model 1 and Model 2 (from left to right).

After the definition of all the parameters, the simulations were performed. The band plots were obtained using the post-processing mode and analyzed for displacement and effective stress. The list of results was exported to a txt. format, and then imported to Excel for data analysis.

3.4 Digital Image Correlation

Digital Image Correlation (DIC) is a non-invasive optical method initially developed to calculate the flow of fluids and surface strain distribution in materials using one camera (2D-DIC). Posterior studies proposed the use of two cameras to have a full-field measurement of models and obtain 3D images of the model (3D - DIC). The comparison with FEM results is then facilitated [18, 52].

The DIC method uses a random speckle that is previously painted in the models and matches points precisely. The speckle is normally a mixture of white and black which results in a grey pattern. With the selection of a square subset in a reference image is possible to locate the same subset in the deformed image. The two centers of the subsets are corresponding points since the speckle in the two images remains the same. Using the distance between the center of the reference and another point in the subset, it is possible to calculate the displacement and deformation associated. In the equation of figure 3.10, $f(x_i,y_i)$ is the position of a point in the reference image that can be related to the position of a point in the deformed area $g(x'_i,y'_i)$, with two factors used to compensate the difference caused by illumination (r_0 and r_1) [18].

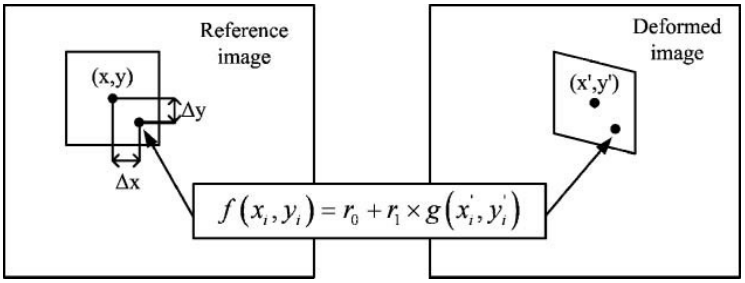

Figure 3.10: Principle of digital image correlation [18].

In 3D-DIC, the one used in this study, the acquisition of images is made using two cameras. The simplified workflow includes the following steps: preparation of the models, camera calibration, image acquisition, image correlation calculation, 3D reconstruction, and calculation of variables [18].

There are several methods to study the biomechanical behavior of prostheses. The advantage of 3D-DIC is its ability to provide a full-field and continuous analysis of a model, with the acquisition of several images during the compression or traction. However, this method has certain limitations such as the application of a satisfactory speckle pattern, involuntary changes in lighting, and replication of in vivo conditions. Although the high number of improvements made in the last few years, it is still hard to simulate the oral conditions and predict the clinical behavior of a prosthesis [50, 53].

3.5 Experimental Preparation

3.5.1 Models

The samples of the 3D models used in the simulations were obtained, as previously explained, with Additive Manufacturing (AM) and Subtractive Manufacturing (SM) techniques. Only PMMA had two samples (one of each method):

- Fabricated through SM: PEEK, PEKK, PMMA, Trilor;
- Fabricated through AM: OXPEKK, PMMA, ABS, HIPS.

Two different types of AM techniques were used: Fused Deposition Modeling (FDM), that is available in the Laboratory of Materials Processing; Selective Laser Sintering (SLS), provided by the enterprise Oxford Performance Materials (OPM).

Along with the frameworks, complete models were also obtained in all the materials. The materials printed with FDM process showed superficial roughness and less rigor in the definition of small features (figure 3.11). For this reason, the

3D printed frameworks made of ABS, HIPS and PMMA were not used, and these materials were only tested in the model of complete prostheses. Depicted in the next pictures are some of the structures studied (figures 3.11, 3.12, 3.13, 3.14). PEEK and PMMA are not represented for lack of acceptable photos. ABS and HIPS, the materials that weren't studied in the simulations, have a modulus of elasticity of 2.5 and 1.9 GPa, respectively.

(a) **(b)**

Figure 3.11: (a) Complete prostheses obtained with FDM: ABS, HIPS and PMMA (bottom to top); (b) On top, an approximation of the PMMA prosthesis and of the HIPS on the bottom. The lines of impression are more visible on the bottom photo. The same pattern can be seen in the ABS printed prosthesis.

In total, five frameworks and eight complete prostheses were studied. In the framework it was necessary to assemble links, as presented in figure 3.12a, to ensure the fixation protocol. After that, with a torque wrench and a 1.2mm hexagonal driver, the multi-unit and the rest of the implant were screwed. The structure obtained can be seen in figures 3.13a and 3.14a.

(a) **(b)**

Figure 3.12: (a) Framework and (b) complete prosthesis made of the resin Trilor. On the framework, it is possible to see the links attached.

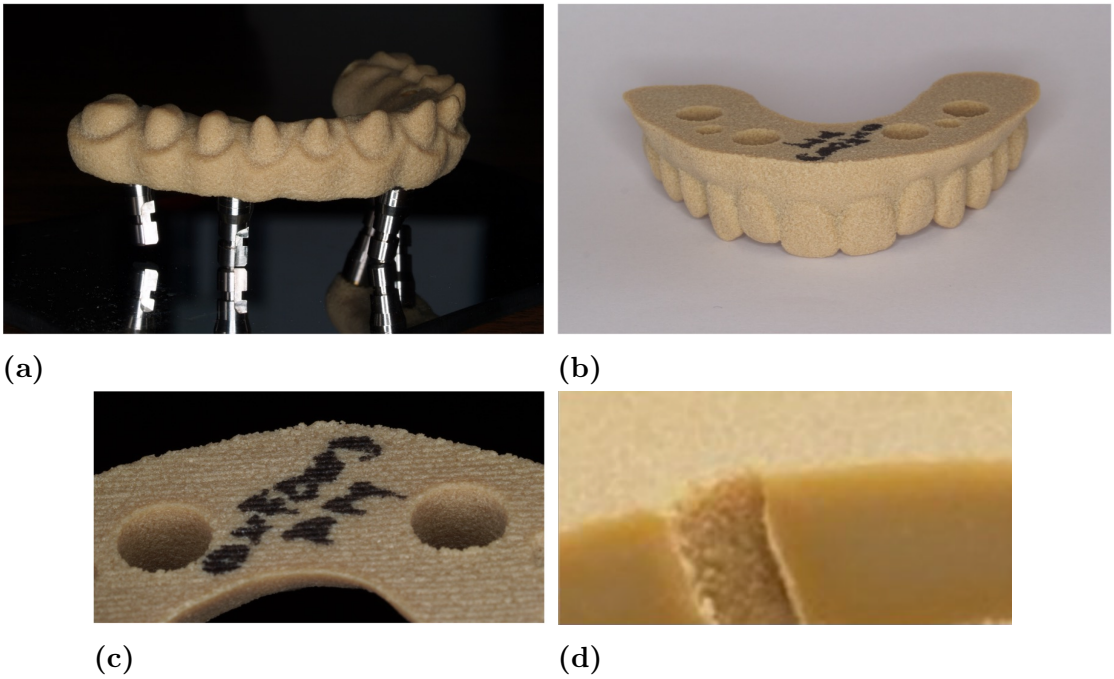

(a) **(b)**

(c) **(d)**

Figure 3.13: Models made of OXPEKK. On the two last photos, approximations of the prosthesis: (c) Some lines are visible on the bottom of the structure; (d) On the inside, a cut revealed a compact surface [6].

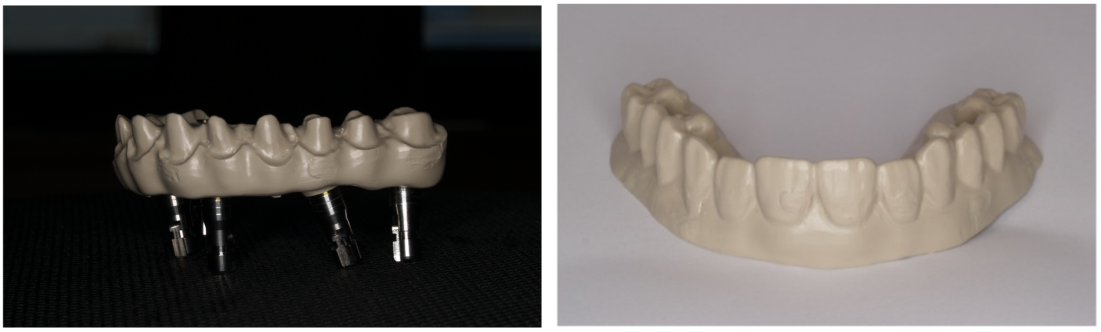

(a) **(b)**

Figure 3.14: (a) Framework and (b) complete prosthesis made of PEKK.

To fix the models with minimal experimental errors, supports were created using SolidWorks®. For the framework (figure 3.15a) was necessary a container to pour a bone simulating resin. This component was printed in Polyethylene Terephthalate Glycol (PET-G) and is the black part of the structure. The blue supports were created to ensure the same protocol of implants fixation for all frameworks. These supports were made of Polylactic Acid (PLA). For the complete prosthesis (figure 3.15b), the same was applied: blue supports made of PLA and a white base of PET-G, which are two materials widely used to print structures using FDM. This step was made with the help of a scholarship student, Nuno Cruz, from the Ap-

plied Biomechanics Laboratory based in ISEC ("Instituto Superior de Engenharia de Coimbra").

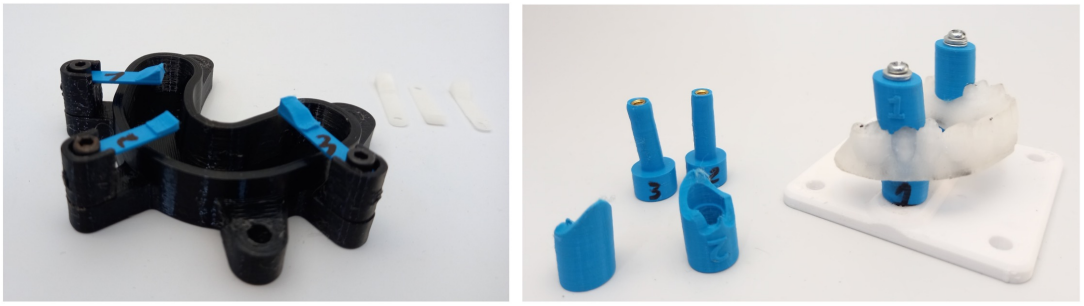

(a) **(b)**

Figure 3.15: Printed supports for the (a) framework and (b) complete prosthesis.

The printed support for the complete prosthesis seen in figure 3.15b needed to be replaced because the retention of the structure was not ideal and induced a lot of movement. Instead, it served as a reference for the fabrication of a metal substitute. A base to fix both of the supports was also milled in metal, with four central holes made for M5 screws. The complete prosthesis was fixed with M7 screws and nuts. In addition, the charge plate was made of metal with a center to fix an M12 screw. These metal components can be seen in figure 3.16.

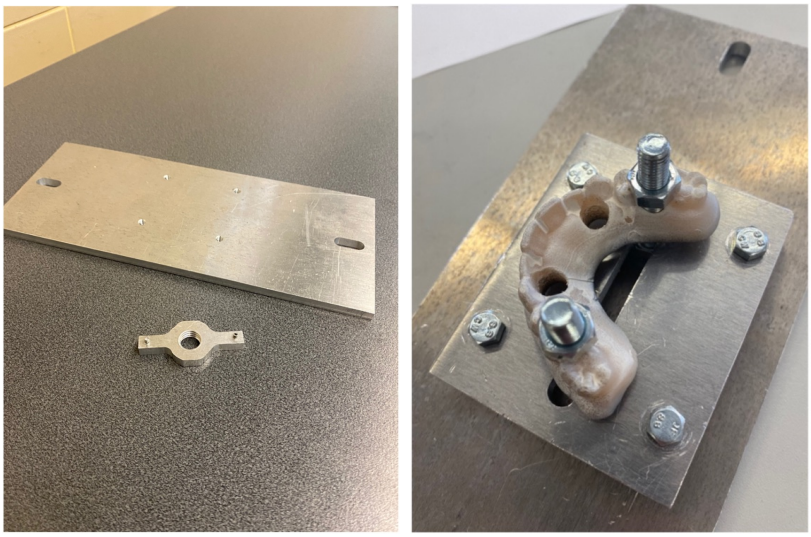

(a) **(b)**

Figure 3.16: Metal parts: (a) On top, the base for both the supports with the four holes made for M5 screws and, on the bottom, the charge plate; (b) Complete prosthesis fixed in the support with M7 screws and nuts.

To simulate the bone and support the structure, a resin was injected into the container (figure 3.17a). The material, Technovit® 4000, was previously tested and

used in other similar biomechanical studies because it is a fast curing resin with low shrinkage properties that decrease the stress induced to the implants [50]. This material has a modulus of elasticity of about 2-2.2 GPa [54]. After the curing and the adhesion were complete, the excess material was removed using a cutting device (figure 3.17b).

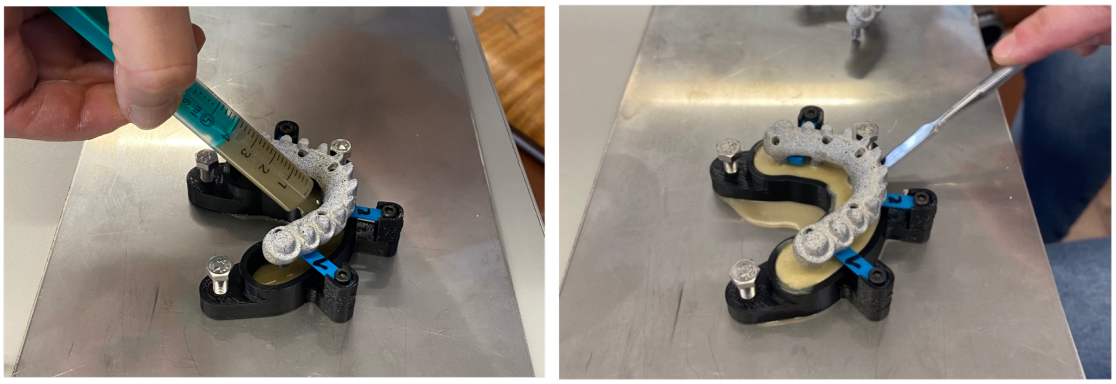

(a) **(b)**

Figure 3.17: Technovit® 4000 setting: (a) Injection; (b) Removing the excess.

Before the experimental tests, all the samples need to be coated with the pattern that allows the use of the digital image correlation method. To obtain the speckle, a homogeneous layer of white ink is applied and then a pulverization of black ink. An approximation of a framework is pictured in figure 3.18, where the pattern is visible.

Figure 3.18: Example of speckle in a framework.

3.5.2 Experimental setup

Two high-speed cameras are positioned on a tripod to capture the images of the experiment. Connected to the cameras is a computer with the software VIC-3D 2010 (Correlated Solutions®), that allows the assessment and process of the

pictures. Natural light isn't enough in this type of study, so illumination devices are placed in strategic places to prevent errors related to changes in lighting.

Before taking images and position the samples, a calibration is necessary. This step was made using a dot grid with defined spaces between the dots, in this case, a 12x9 dot grid with 4mm between the dots. Acquisition of multiple images of the grid in different positions allows the calibration of the system and the definition of a relationship between the camera coordinates and the real coordinates of the model. After running the calibration photos, a score shows the error between the real position and the position calculated. The smaller the error number, the better calculation of the positions.

The samples were mechanically tested using a traction/compression machine available in the Laboratory of Mechanical Characterization, Shimadzu® Autograph (Shimadzu® Corporation), that presents a maximum load capacity of 5kN. This machine is controlled by a computer with a specific software, TRAPEZIUM X (Shimadzu® Corporation), where the compression cycles were defined. The maximum load of compression was 200N, with a stop of 3 seconds in the 100N load, to facilitate the acquisition of images. A minimum of 3 acquisitions was performed in each sample. Figure 3.19 presents all the components of the experimental setup.

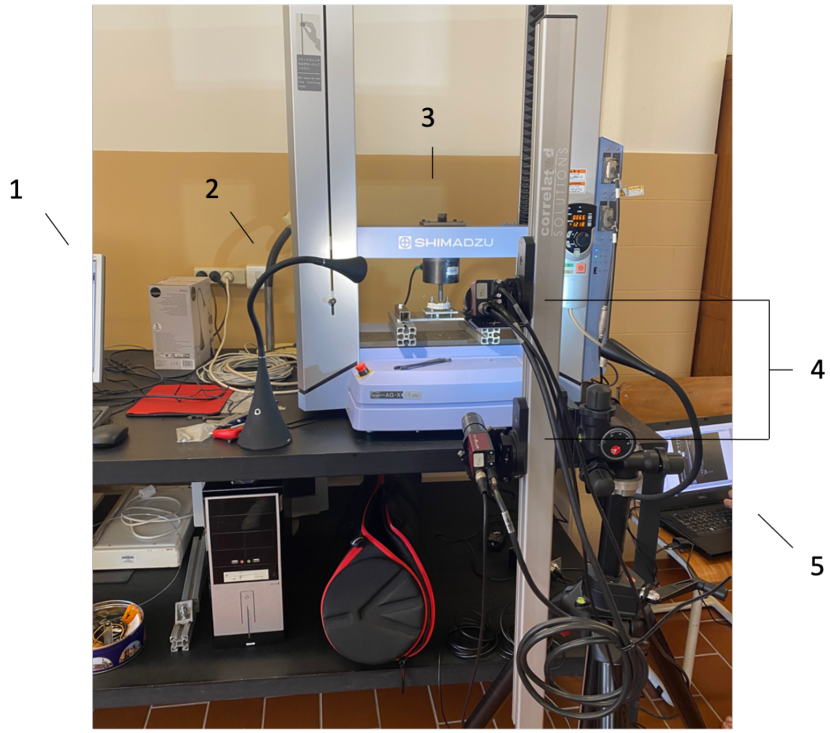

Figure 3.19: Experimental setup: 1 - Computer with the software TRAPEZIUM X; 2 - Lighting; 3 - Traction/Compression machine Shimadzu® Autograph; 4 - Cameras on the support tripod; 5 - Computer with the software VIC - 3D.

The metal bars under the sample were used to position the system in the center of compression. In figure 3.19 it is also visible that the cameras are positioned in vertical to improve the visualization of the models. The images will appear with a rotation, which means that our coordinate system will rotate too. This point is important for the presentation of the results: the vertical displacement of the load cell will correspond to the U displacement in the VIC software (see figure 3.20).

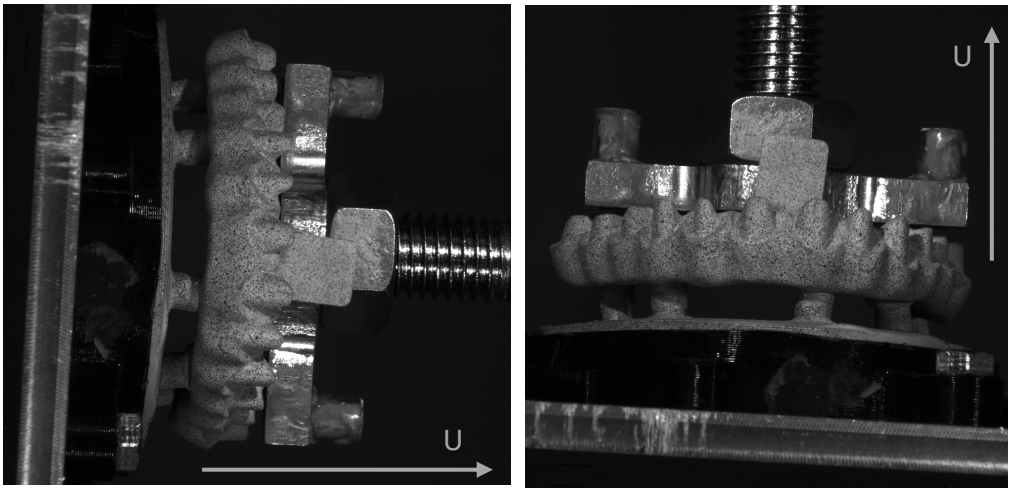

(a) **(b)**

Figure 3.20: Images obtained in the software VIC-3D: (a) Original image with the direction of the U displacement represented; (b) Image with rotation, in which is visible that the U displacement of the software corresponds to the vertical displacement of the load cell.

The compression of the complete prostheses was established using a spherical surface on the tip of a screw. Two different points were compressed: the incisors and the molar. Figure 3.21 shows the first test position.

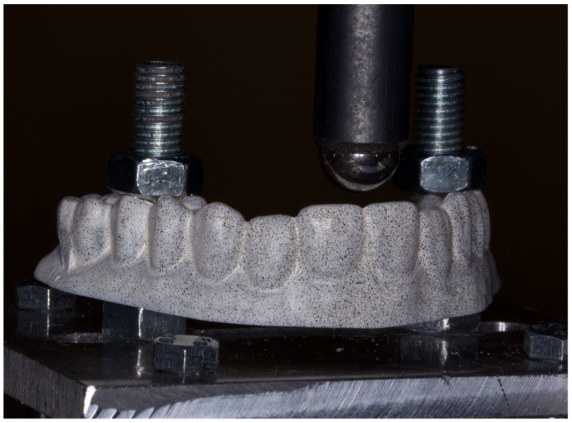

Figure 3.21: Compression of the complete prostheses in the incisors. Note the spherical surface used for the compression.

For the tests in the frameworks, two M12 screws were used, one attached to the machine and the other to the charge plate, previously shown in figure 3.16a, or to a nut. Between the two heads of the screws, a ball joint was positioned to ensure the load was always vertical. The compression was also made in two positions: the incisors and the premolars (with frontal view and lateral view).

After the acquisition of speckle images of the tests, the next step was to perform the VIC analysis. The calibration images and the speckle images were imported to the software VIC-3D to proceed with the analysis. In the reference image (image of the model with no compression), an area of interest was selected to be analyzed. This area remains the same for the next pictures, in which the displacement variation and other variables were calculated.

4

Results and Discussion

Throughout this chapter, the results of the numerical and experimental study are presented and discussed.

As stated in previous chapters, the first step was the numerical analysis. This step aimed to obtain a brief initial characterization of the biomechanical behavior of some of the materials of this study, using a simple static simulation. The comparison was also made with conventional materials. Data was collected using the post-processing resource of ADINA® and then processed with Excel and MATLAB (MathWorks®). The variables studied were the global magnitude of displacement and the effective stress (equivalent to the von Mises stress). On the framework study, the results of the framework and the links were analyzed separately. The images and the values of the links are presented in appendix A to facilitate the reading and the comparison of the results for the frameworks. The maximum limits used for the color scale were the same for the different materials and are as follows:

- Framework: $1x10^{-7}$ m for the displacement magnitude and $6x10^{6}$ Pa for the effective stress;

- Links: $2x10^{-6}$ m for the displacement magnitude and $2x10^{7}$ Pa for the effective stress.

In the experimental study, the goal was to test the frameworks in different loading positions and also the model of a complete prosthesis. The data was collected in the software VIC-3D and then processed with Excel. The variables studied were the displacement and the principal strains. In this case, a region of interest was selected to obtain the mean values of the variables to study.

4.1 Numerical Study - Model 1

It is evident from the images of the first simulations that there are differences between the frameworks with lower and with higher Modulus of Elasticity (E), which can be seen in figures 4.1 and 4.2. As expected, displacements are higher in the frameworks made of polymeric materials; nevertheless, the distribution is quite similar among materials. Table 4.1 compiles the values of mean, maximum, and minimum displacement magnitude. We can see that PMMA has the highest values of maximum and mean displacement, followed by OXPEKK, PEEK, and PEKK. The maximums of the polymers are significantly higher than the ones obtained on the other materials, which can become a problem. For example, PMMA and OXPEKK, the materials with higher displacement, have a maximum respectively 22.5 and 19 times bigger than the maximum of Co-Cr. The ANOVA test confirms that there are statistically significant differences between the mean values ($p<0.001$).

Contrary to what was observed in the displacements, figure 4.2 reveals a higher extension of effective stress in the frameworks with higher young modulus, that spreads from the load application site to the center of the structure. Trilor, the FRC material, presents an intermediate behavior. Table 4.2 shows the discrepancy between the maximums of the metal/metal alloy structures and the other ones. Co-Cr reaches a maximum 5.6 times bigger than PMMA and 5.3 than OXPEKK. Also taking Co-Cr for reference, the mean value of the effective stress of the framework can be reduced by more than 40% with the use of any of the polymers tested and by 30% with the use of Trilor. The ANOVA test confirms that exist statistical significant differences between the materials ($p<0.001$).

The images of these simulations also show that there is some asymmetry in the distribution of both the displacement magnitude and the effective stress, with the right side of the framework being more affected than the other. This can be the result of the asymmetrical distribution of the holes for the implants.

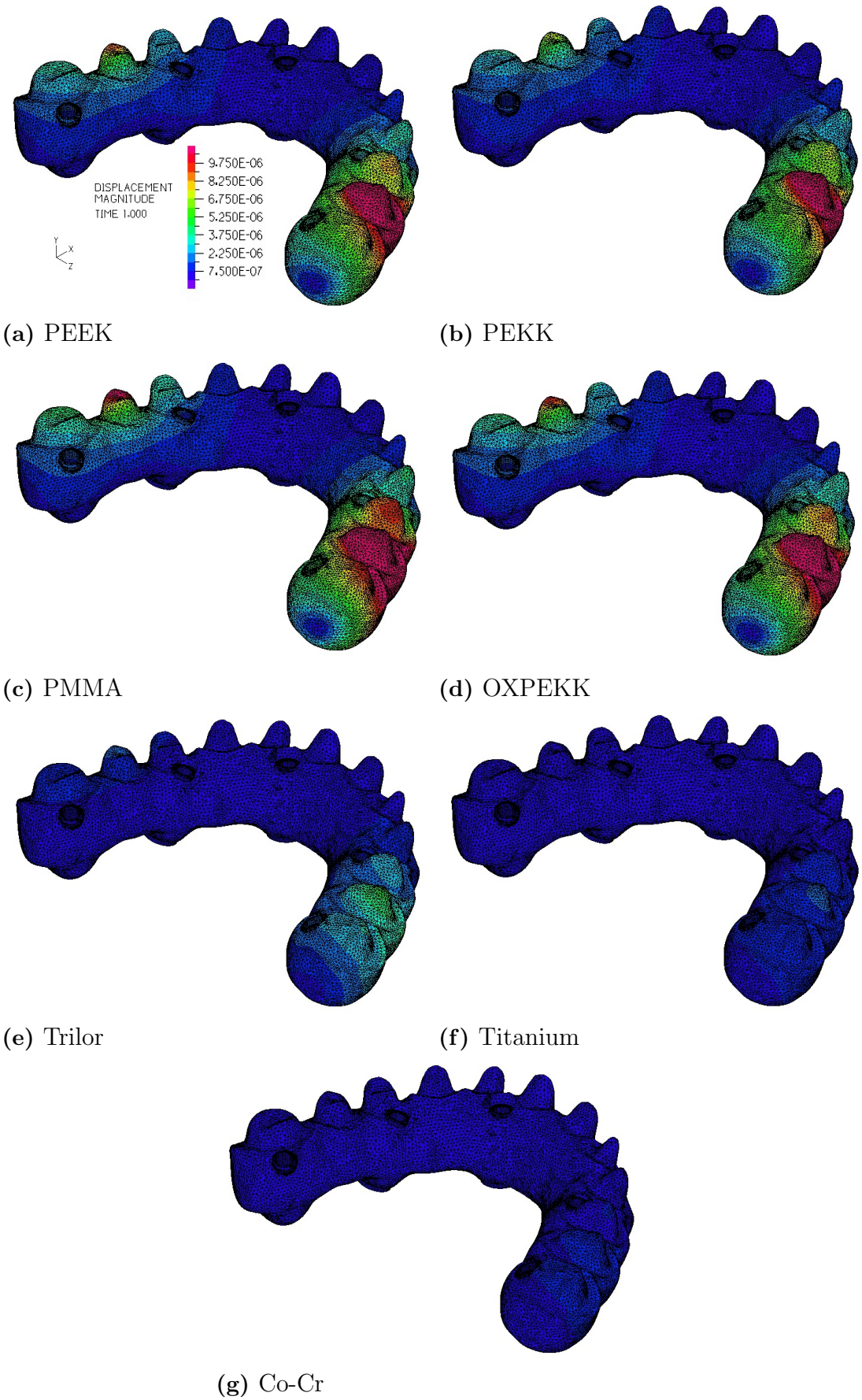

(a) PEEK **(b)** PEKK

(c) PMMA **(d)** OXPEKK

(e) Trilor **(f)** Titanium

(g) Co-Cr

Figure 4.1: Displacement magnitude of Model 1.

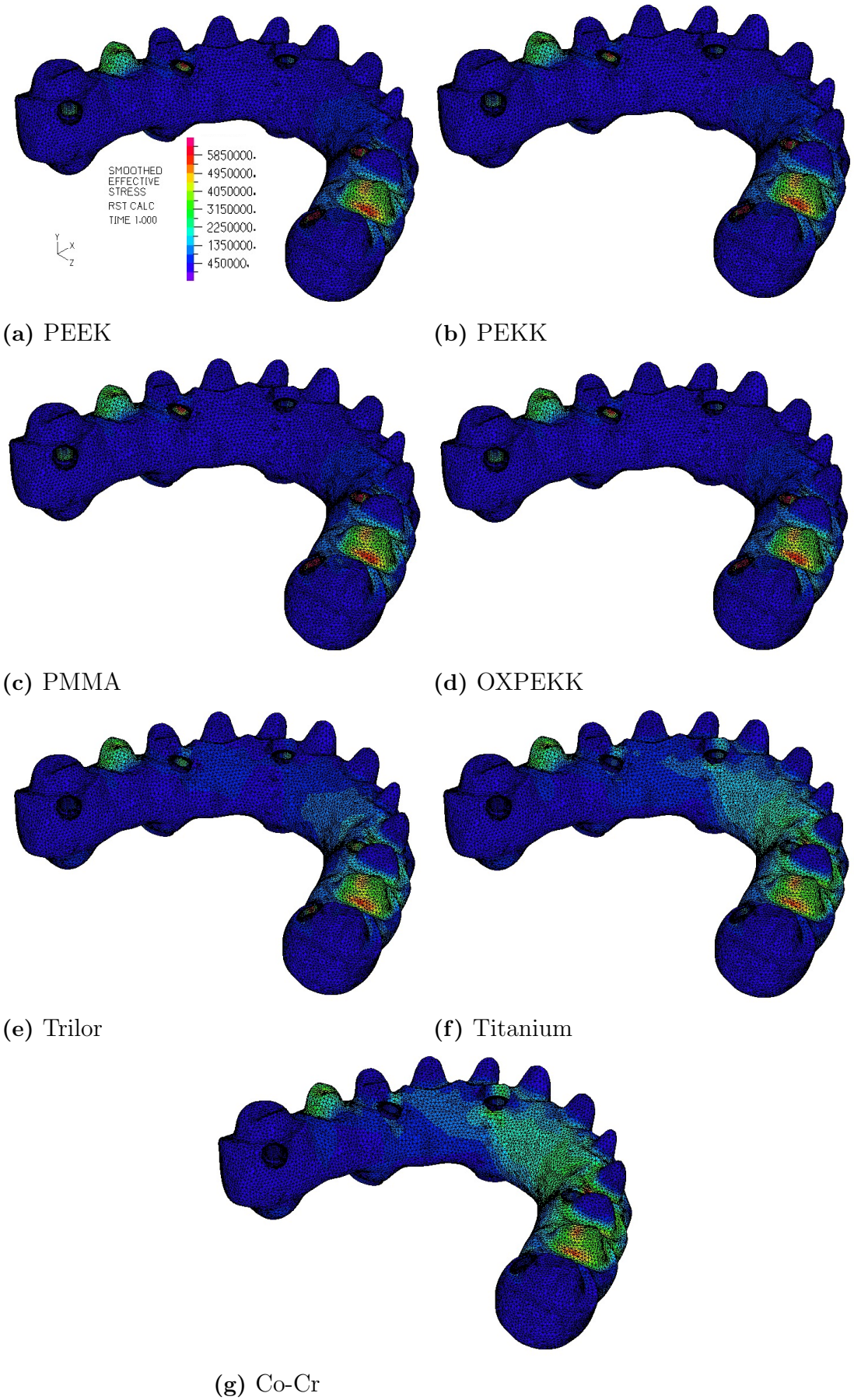

(a) PEEK

(b) PEKK

(c) PMMA

(d) OXPEKK

(e) Trilor

(f) Titanium

(g) Co-Cr

Figure 4.2: Effective stress of Model 1.

Table 4.1: Mean, standard deviation and extreme values of displacement magnitude for the framework of Model 1.

Materials	Mean ± sd (μm)	Maximum (μm)	Minimum (μm)	ANOVA test
PEEK	2.203 ± 2.776	19.720	0.001	
PEKK	1.912 ± 2.366	16.508	0.001	
PMMA	2.710 ± 3.505	25.435	0.001	
OXPEKK	2.356 ± 2.995	21.457	0	F(6,553140)=16955.9660,
Trilor	0.710 ± 0.790	4.741	0.002	p<0.001
Titanium	0.319 ± 0.330	1.718	0.001	
Co-Cr	0.227 ± 0.228	1.130	0.001	

Table 4.2: Mean, standard deviation and extreme values of effective stress for the framework of Model 1.

Materials	Mean ± sd (MPa)	Maximum (MPa)	Minimum (MPa)	ANOVA test
PEEK	0.537 ± 0.704	9.312	0.001	
PEKK	0.549 ± 0.710	9.798	0.002	
PMMA	0.523 ± 0.700	8.579	0.001	
OXPEKK	0.532 ± 0.702	9.090	0.001	F(6,553140)=4050,2583,
Trilor	0.660 ± 0.753	12.667	0.002	p<0.001
Titanium	0.834 ± 0.802	36.882	0.005	
Co-Cr	0.942 ± 0.852	48.234	0.006	

4.2 Numerical Study - Model 2

As previously referred, Model 2 aimed a better replication of the reality of the frameworks for ISFPs to compare with the first simulations. For this, the same scale was used to observe visual differences. The results for the displacement (figure 4.3) show similar distributions of displacements to that of Model 1, but with more nodes with higher values (depicted in red/magenta in the polymers). In the Trilor and Titanium images is visible an increase of incidence in the right area shown in green and blue, respectively. In the effective stress images (figure 4.4), we can see that the same critical areas are affected. The most visible difference is the increase of the green color in the Titanium and the Co-Cr frameworks which indicates bigger values.

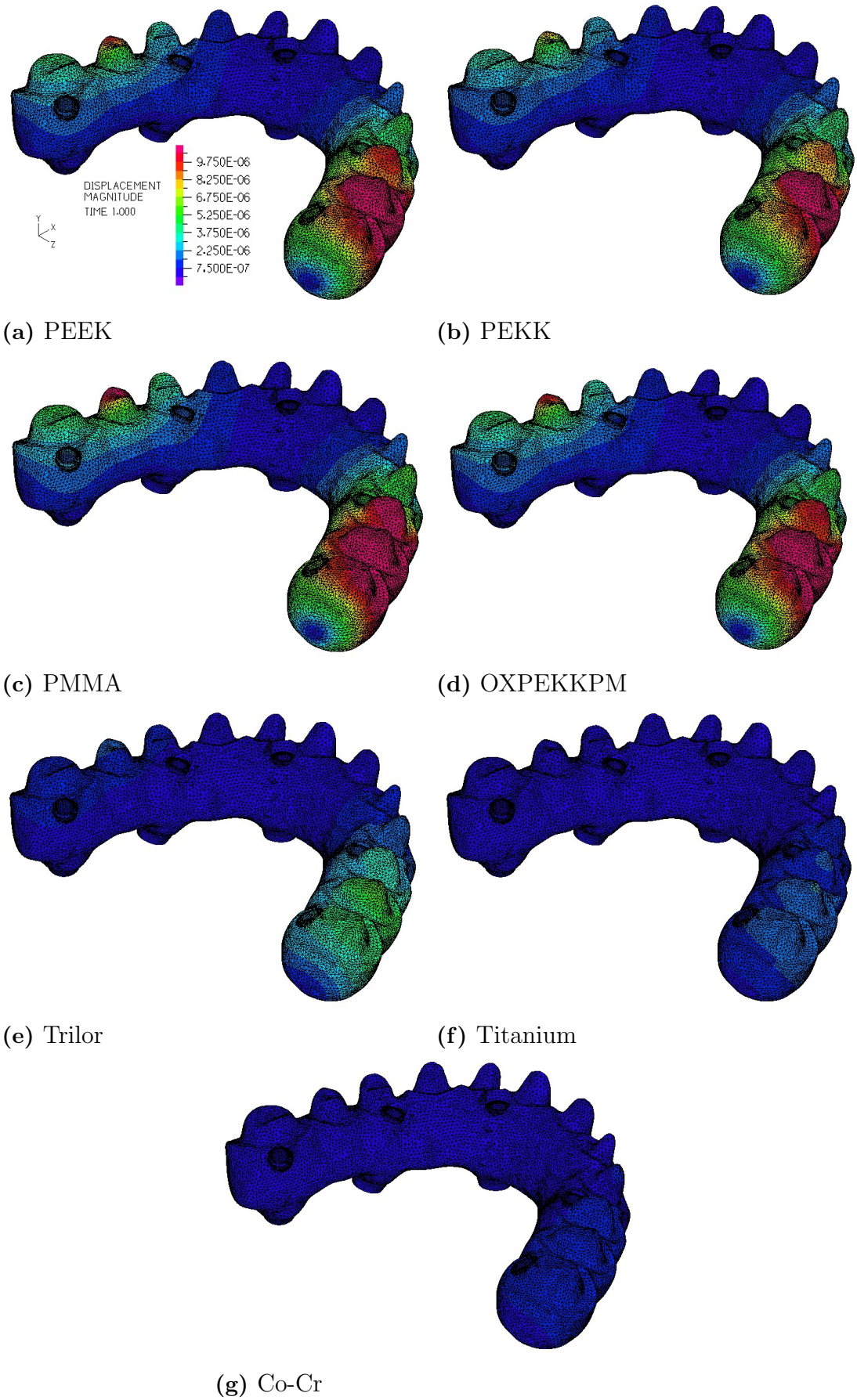

(a) PEEK **(b)** PEKK

(c) PMMA **(d)** OXPEKKPM

(e) Trilor **(f)** Titanium

(g) Co-Cr

Figure 4.3: Displacement magnitude of Model 2.

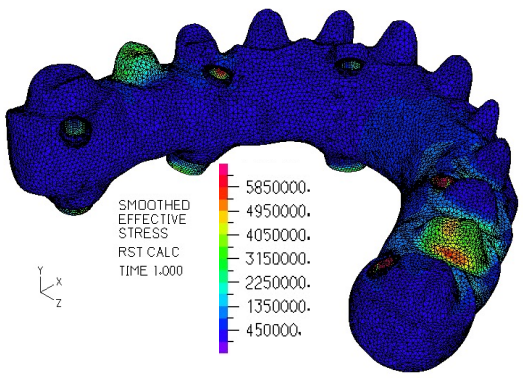

(a) PEEK

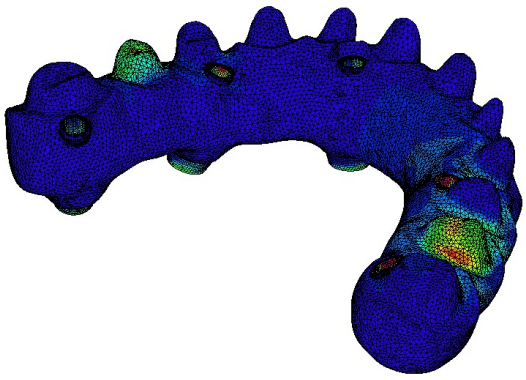

(b) PEKK

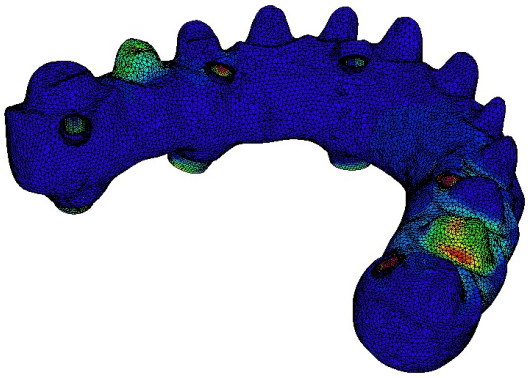

(c) PMMA

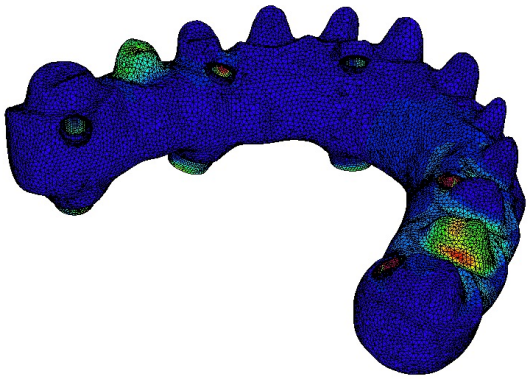

(d) OXPEKK

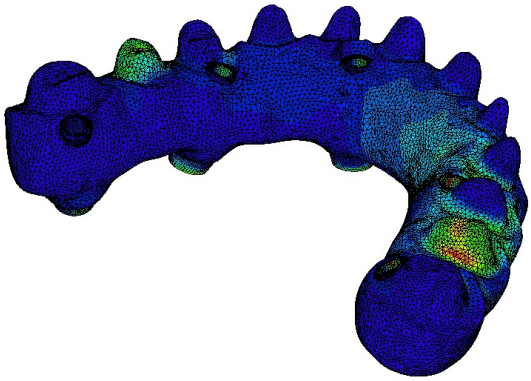

(e) Trilor

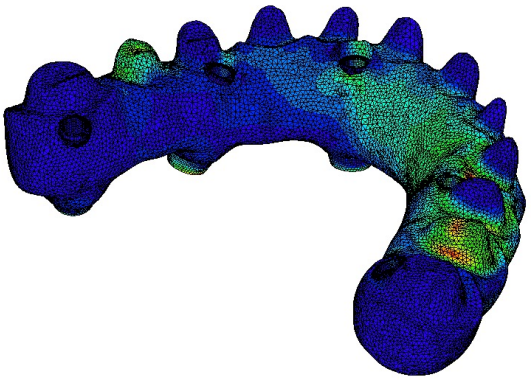

(f) Titanium

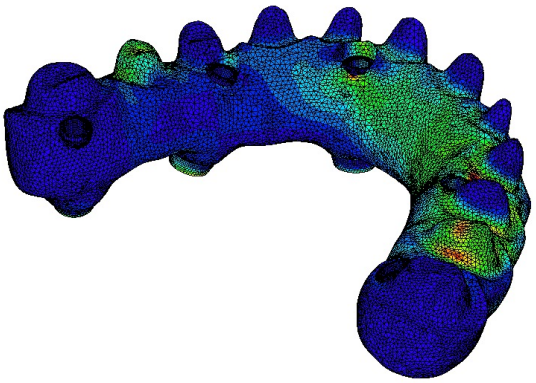

(g) Co-Cr

Figure 4.4: Effective stress of Model 2.

The mean, maximum, and minimum of displacement calculated for each material are presented in tables 4.3 and 4.4. The mean and maximum values of displacement showed a slight increase when compared to the results of Model 1 but maintained the same pattern. The means of effective stress also increase in all the materials. The notorious difference is the decrease of the maximums of Titanium and Co-Cr, this last one in more than 10 MPa. Despite that, these values are still significantly higher than the other maximums, at least 2.5 to 3 times bigger. Both the two ANOVA tests show that statistically there are significant differences between the results ($p<0.001$).

Table 4.3: Mean, standard deviation and extreme values of displacement magnitude for the framework of Model 2.

Materials	**Mean ± sd (μm)**	**Maximum (μm)**	**Minimum (μm)**	**ANOVA test**
PEEK	2.726 ± 3.258	22.133	0.010	
PEKK	2.411 ± 2.831	18.786	0.011	
PMMA	3.266 ± 4.009	28.024	0.010	
OXPEKK	2.890 ± 3.485	23.934	0.016	F(6,553140)=17352.1698,
Trilor	1.017 ± 1.092	6.066	0.004	p<0.001
Titanium	0.466 ± 0.469	2.304	0.003	
Co-Cr	0.325 ± 0.316	1.497	0.005	

Table 4.4: Mean, standard deviation and extreme values of effective stress for the framework of Model 2.

Materials	**Mean ± sd (MPa)**	**Maximum (MPa)**	**Minimum (MPa)**	**ANOVA test**
PEEK	0.557 ± 0.706	10.380	0.002	
PEKK	0.572 ± 0.712	10.955	0.002	
PMMA	0.540 ± 0.670	9.520	0.002	
OXPEKK	0.550 ± 0.703	10.111	0.002	F(6,553140)=6503.7503,
Trilor	0.718 ± 0.769	13.653	0.003	p<0.001
Titanium	0.950 ± 0.859	33.9613	0.004	
Co-Cr	1.083 ± 0.921	34.942	0.004	

To compare the behavior of the two models and to better understand the distribution of the displacement magnitude and the effective stress, the frequency distribution graphics of both variables were obtained and are displayed in figures 4.5, 4.6, 4.7 and 4.8.

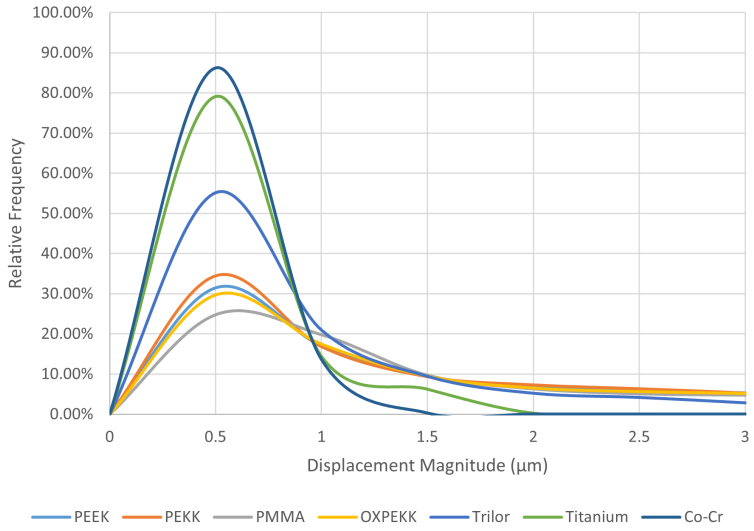

Figure 4.5: Distribution of displacement magnitude values for the framework of Model 1.

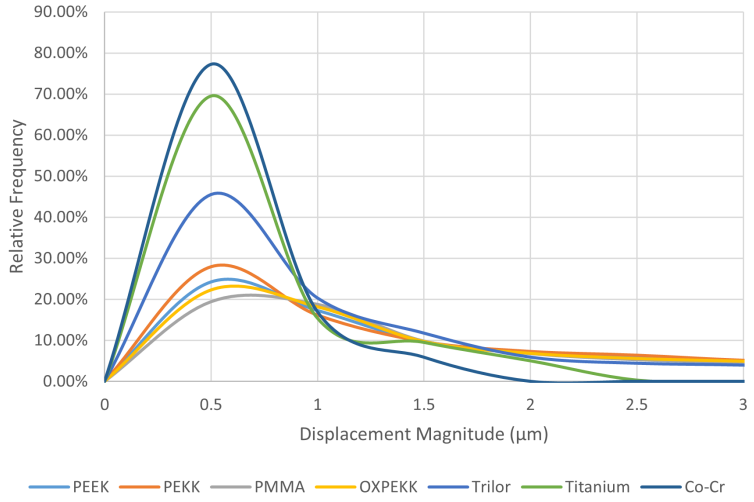

Figure 4.6: Distribution of displacement magnitude values for the framework of Model 2.

In figures 4.5 and 4.6, it is visible that frameworks of classic material have a higher percentage of volume with smaller level displacements compared to the rest of the materials. The distribution curves of polymeric material are wider than the other curves, which means that the loading effect is less localized. It is also possible to conclude that the presence of the multi-units to perform the implant attachment leads to higher displacements.

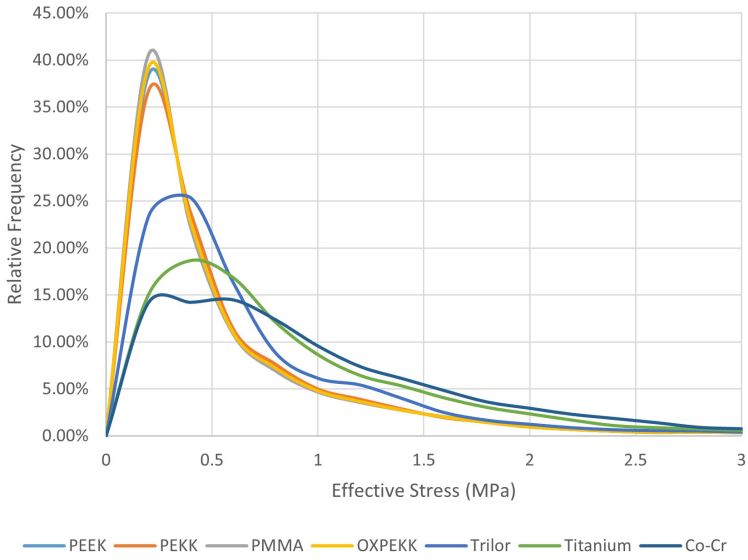

Figure 4.7: Distribution of effective stress values for the framework of Model 1.

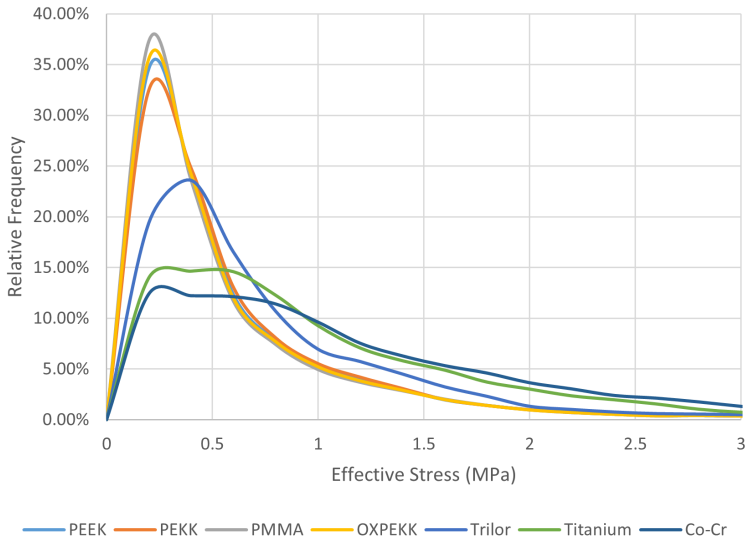

Figure 4.8: Distribution of effective stress values for the framework of Model 2.

The distribution of stress pictured in figures 4.7 and 4.8 shows a pattern similar to what was previously described. The upgrade led to a general decrease in the peaks of stress and consequently the incidence of higher values. A flattening of the line is visible in Titanium, which indicates a wider distribution of values.

The variables were also analyzed using boxplots, displayed in figures 4.9, 4.10, 4.11 and 4.12. In this statistical analysis, the outliers were omitted to allow better visualization of each quartile.

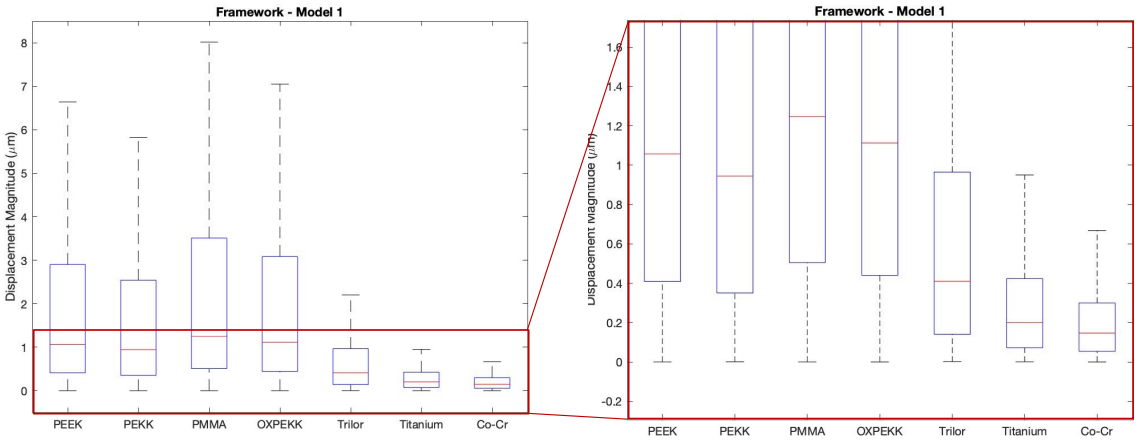

Figure 4.9: Boxplot of the displacement magnitude in the framework of Model 1. On the right, an approximation of the median.

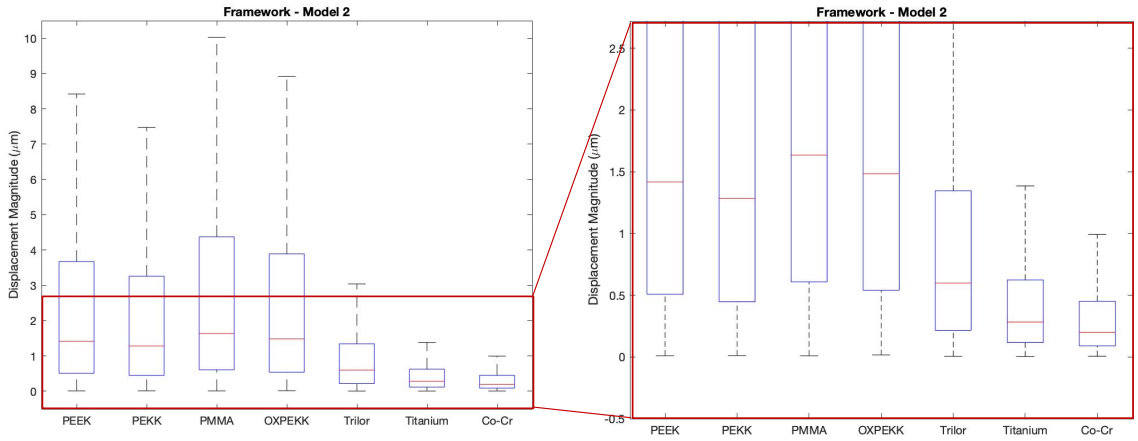

Figure 4.10: Boxplot of the displacement magnitude in the framework of Model 2. On the right, an approximation.

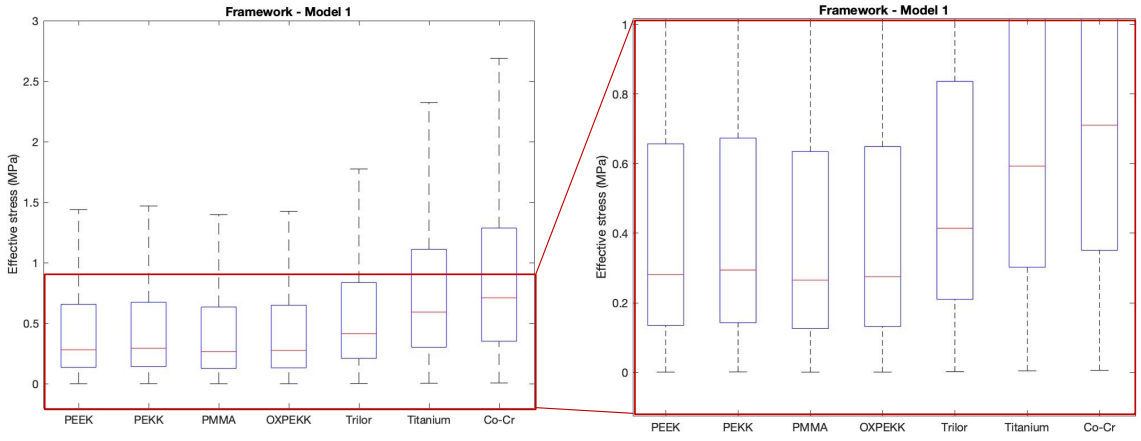

Figure 4.11: Boxplot of the effective stress in the framework of Model 1. On the right, an approximation.

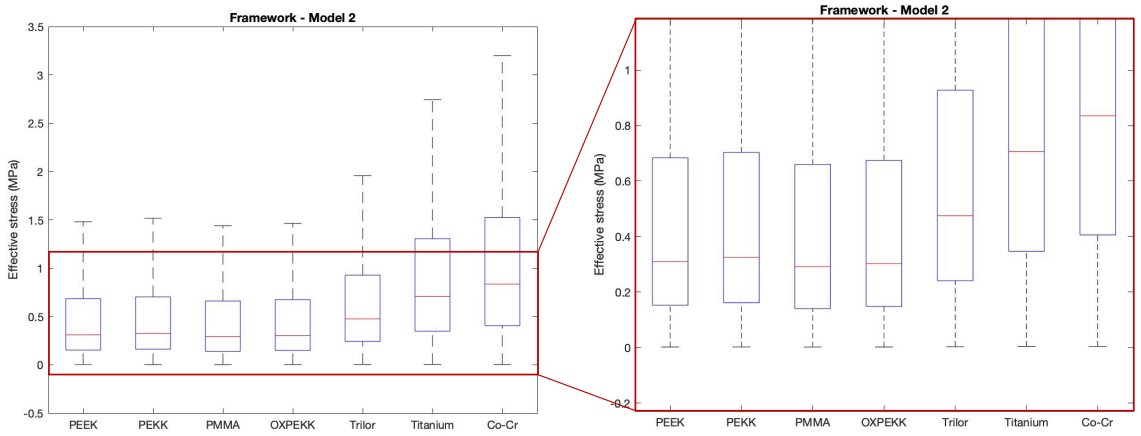

Figure 4.12: Boxplot of the effective stress in the framework of Model 2. On the right, an approximation.

The boxplots confirmed the wider range of values in the polymeric materials. It is also possible to observe an increase of the median, the third quartile, and the superior limit from Model 1 to Model 2, most visible in the displacement magnitude graphics.

The analysis of the links is presented in appendix A. The links of Model 1 (appendix A.1) present higher displacement magnitude in the polymeric frameworks, which can result from the movement implied by the structure. Likewise, higher values of stress are displayed when polymers are used. This can be explained by the fact that the links are made of titanium and are more rigid than the framework material. Model 2, in accordance to what happened in the framework, shows the same pattern of Model 1 (see appendix A.2): wider distribution of values and increase of

the mean values. An asymmetry is also visible in both models, with the links in the right side presenting higher values.

We can conclude that both simulations presented identical critical zones and results. The materials can be sorted as follows, from highest to lowest mean value of each variable:

- Displacement magnitude: PMMA, OXPEKK, PEEK, PEKK, Trilor, Titanium, Co-Cr;
- Effective stress: Co-Cr, Titanium, Trilor, PEKK, PEEK, OXPEKK, PMMA.

4.3 Experimental Study - Framework

As stated in the beginning of this chapter, the models were tested in different positions and a region of interest was selected in each one. Figure 4.13 shows the regions studied in the framework.

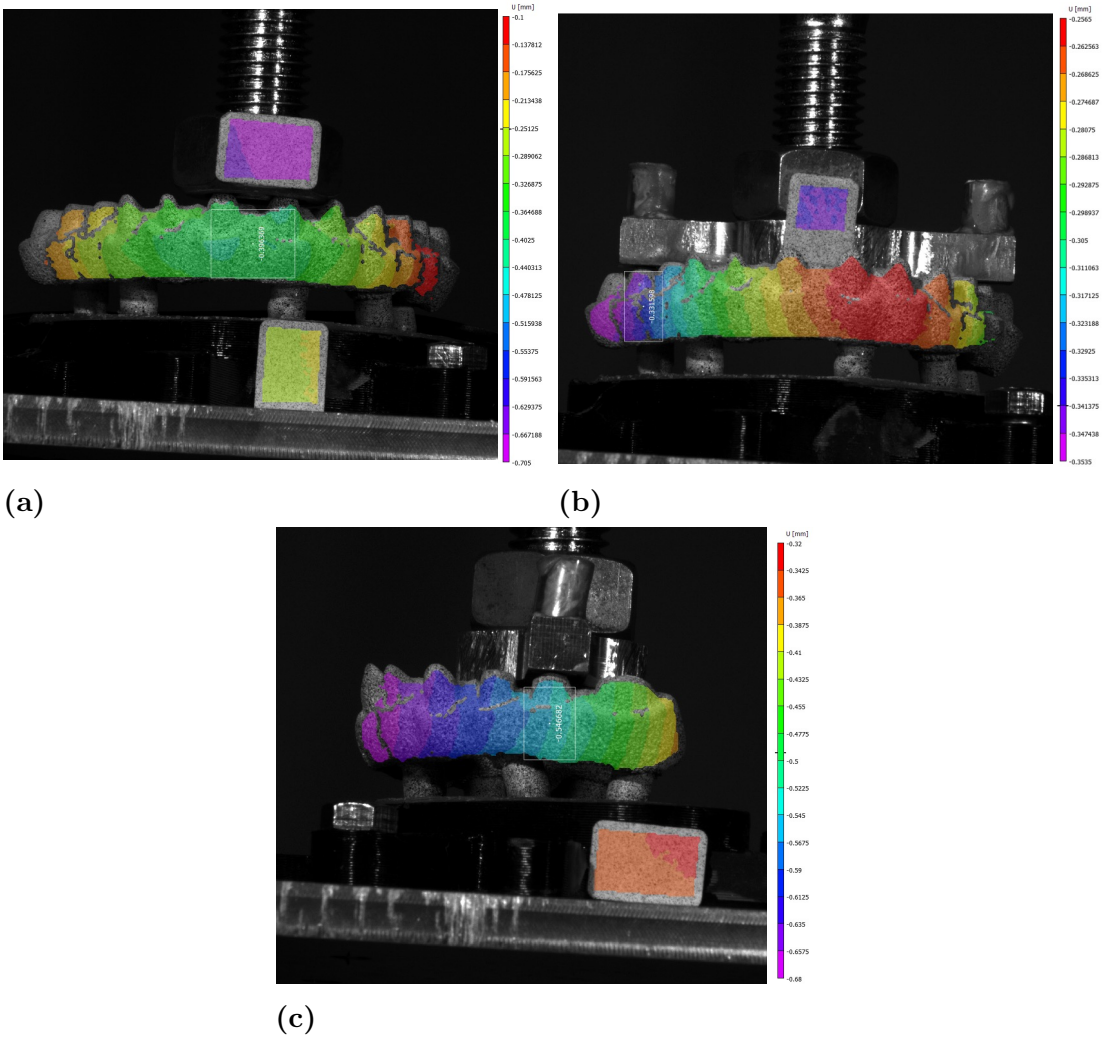

Figure 4.13: Regions of interest represented by a white rectangle and selected in each position: (a) Incisors, (b) Premolars (frontal view) and (c) Premolars (lateral view). All the frameworks represented are made of OXPEKK, and the photos were taken at a 200N load compression. The scales on the right of each picture are automatically generated and different in each position.

Compression of the incisors

The average displacement of the load cell was calculated and compiled in table 4.5. For this, the data from each test were analyzed to delete initial unwanted displacements (that result from the distance of the load cell to the sample) and

also erratic tests (result mainly of slips or misposition of the load cell). The better representation of the displacement obtained for each material was chosen and joined in figure 4.14.

Table 4.5: Average displacement obtained on the Shimadzu machine for the compression of the incisors in the framework.

Materials	Load (N)	Mean (mm)	± Standard Deviation (mm)
PEEK	100	0.8111	0.0229
	200	1.2084	0.0311
PEKK	100	0.6813	0.0825
	200	0.9640	0.1115
PMMA	100	0.8733	0.1000
	200	1.1384	0.1202
OXPEKK	100	0.8436	0.0351
	200	1.1817	0.0448
Trilor	100	0.7399	0.0102
	200	1.0632	0.0096

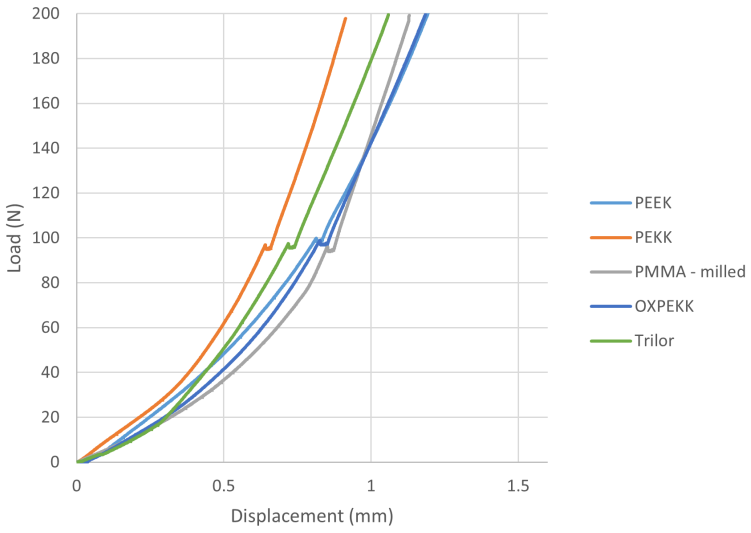

Figure 4.14: Vertical displacement of the load cell of the Shimadzu machine for the compression of the incisors in the framework.

The graphics of displacement show a similar advance when compressed with loads under 20N; when the load increases, the materials show a little divergence. It is visible that PEKK and Trilor present the lowest maximum values, followed by PMMA, OXPEKK and PEEK. PMMA displays the higher displacement when compressed with a 100N load, but when the load increases the displacement rate becomes smaller. PEEK and OXPEKK present a similar behavior, with the highest

maximum values of displacement.

In the software VIC-3D, the mean values of the displacement in the regions of interest were obtained and are presented in table 4.6. Figure 4.15 represents in a diagram the results obtained for the vertical displacement, which can be compared with the results obtained for the load cell.

Table 4.6: Average displacement obtained on the software VIC-3D for the compression of the incisors in the framework.

Materials	Load (N)	U (mm)	± sd (mm)	V (mm)	± sd (mm)
PEEK	100	-0.2534	0.0725	0.0160	0.0179
	200	-0.4233	0.0466	0.0305	0.0060
PEKK	100	-0.2276	0.0124	-0.0573	0.0444
	200	-0.3710	0.0040	-0.0535	0.0467
PMMA	100	-0.0595	0.0247	0.0424	0.0210
	200	-0.1269	0.0221	0.0261	0.0223
OXPEKK	100	-0.2707	0.0906	0.0407	0.0165
	200	-0.4470	0.0924	0.0658	0.0216
Trilor	100	-0.2204	0.0215	-0.0089	0.0334
	200	-0.3709	0.0161	-0.0668	0.0271

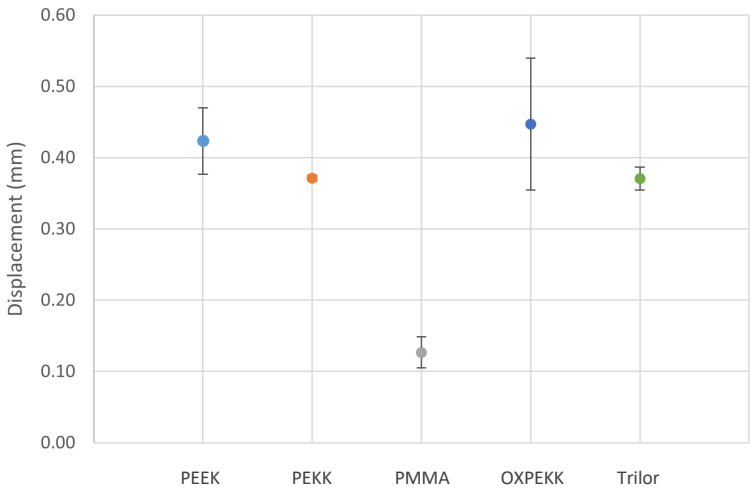

Figure 4.15: Absolute value of vertical displacement (U) in millimeters (mm) obtained on VIC-3D for the compression of the incisors in the framework under a 200N load. The bars in each point represent the standard deviation.

The results reveal that all the maximums of vertical displacement are smaller than the values obtained for the load cell. In figure 4.13a, we can see that the speckled band placed in the load cell shows higher absolute displacement than the compressed incisors. This can be due to some slip of the load cell that induced some unwanted displacement and differences between the values. Despite that, the order

of the material's vertical displacement is similar to the values of the machine: PEEK and OXPEKK present closer values and PEKK and Trilor show lower displacement. The exception is PMMA, which shows a value way lower than expected.

Besides the displacement, the principal strains were obtained, and the results for the first tested position are compiled in table 4.7.

The maximum principal strains, ε_1, represent a positive deformation or tensile strain of the samples. These values are higher in PMMA, followed by PEEK, OXPEKK, PEKK, and Trilor. The minimum principal strains, ε_2, represent the negative deformation or compressive strain of the models. OXPEKK presents the higher value of compressive strain, followed by PMMA, PEEK, PEKK, and Trilor.

Table 4.7: Average value of the principal strains obtained on VIC-3D software for the compression of the incisors in the framework with a 200N load.

Materials	**Load (N)**	ε_1 ($\mu\varepsilon$)	$\pm$ **sd** ($\mu\varepsilon$)	ε_2 ($\mu\varepsilon$)	$\pm$ **sd** ($\mu\varepsilon$)
PEEK	200	1249.9933	246.5275	-2058.4894	184.1569
PEKK		960.7937	211.9865	-1390.0800	457.3629
PMMA		1491.7784	379.3810	-2194.5954	143.0865
OXPEKK		1245.3619	145.3531	-3217.1821	1289.8436
Trilor		536.3377	118.6130	-1289.6686	180.3846

Compression of the premolars (frontal view)

The same process was followed in the other positions of test. The results of the machine are displayed in table 4.8 and figure 4.16. The values obtained in the software VIC-3D are presented in tables 4.9 and 4.10 and figure 4.17.

Table 4.8: Average displacement obtained on the Shimadzu machine for the compression of the premolars in the framework (frontal view).

Materials	**Load (N)**	**Mean (mm)**	$\pm$ **Standard Deviation (mm)**
PEEK	100	0.5751	0.0124
	200	0.8305	0.0589
PEKK	100	0.5968	0.0584
	200	0.8589	0.0524
PMMA	100	0.5549	0.0829
	200	0.7604	0.0992
OXPEKK	100	0.6395	0.0464
	200	0.9556	0.0589
Trilor	100	0.5151	0.0304
	200	0.7335	0.0392

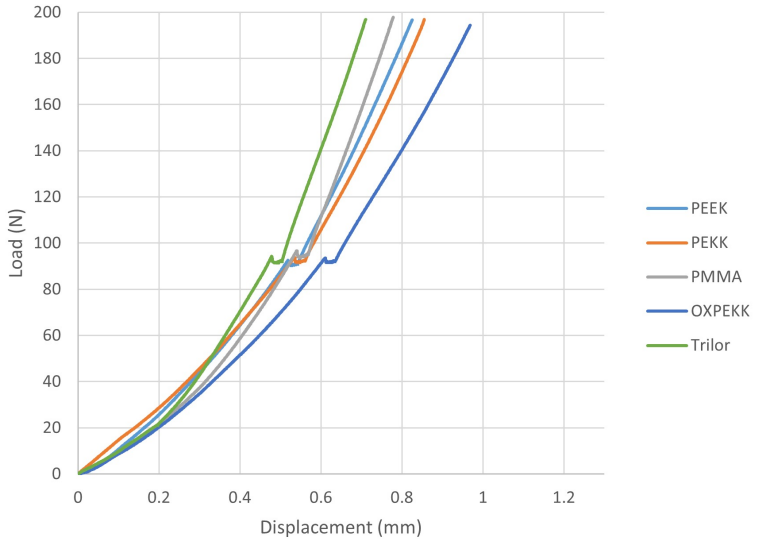

Figure 4.16: Vertical displacement of the load cell of the Shimadzu machine for the compression of the premolars in the framework (frontal view).

In the graphics, some of the initial displacement, close to zero, was removed from all the materials. This initial unwanted movement could be due to small adjustments of the loading device to the position in the initial phase. We can see that OXPEKK presents the highest values of displacement from the beginning. All the materials present small values of displacement, which means that some differences are noted from 100N to 200N and that a small misalignment in the experimental setup can make a big difference.

Table 4.9: Average displacement obtained on the software VIC-3D for the compression of the premolars in the framework (frontal view).

Materials	**Load (N)**	**U (mm)**	**± sd (mm)**	**V (mm)**	**± sd (mm)**
PEEK	100	-0.1464	0.0319	-0.0447	0.0433
	200	-0.2449	0.0566	-0.0579	0.0359
PEKK	100	-0.2198	0.0248	-0.0957	0.0150
	200	-0.3301	0.0255	-0.1304	0.0162
PMMA	100	-0.1086	0.0007	-0.0107	0.0120
	200	-0.2432	0.0173	-0.0076	0.0178
OXPEKK	100	-0.2027	0.0348	-0.0936	0.0648
	200	-0.3504	0.449	-0.1187	0.0591
Trilor	100	-0.1241	0.0453	-0.0269	0.0093
	200	-0.1875	0.0419	-0.0253	0.0038

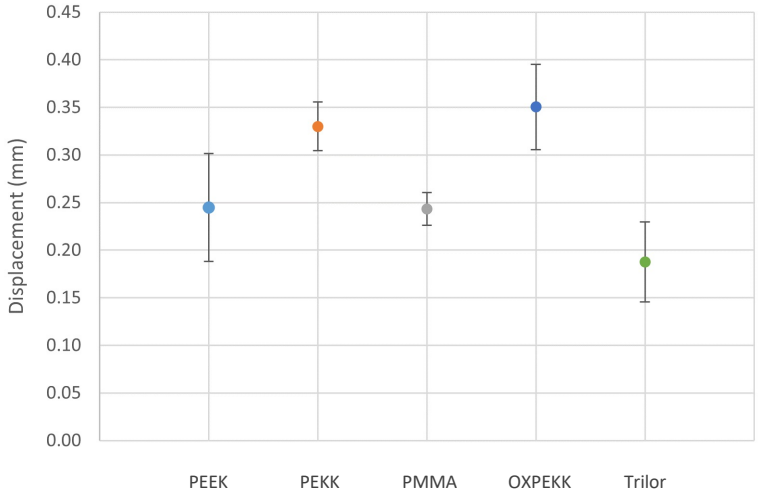

Figure 4.17: Absolute value of vertical displacement (U) in millimeters (mm) obtained on VIC-3D for the compression of the premolars in the framework (frontal view) under a 200N load. The bars in each point represent the standard deviation.

As previously noted, the values obtained in the software are lower than the results of the machine, in this case about three times. Nonetheless, the order of maximum displacement in the materials is the same, which can indicate the existence of a systematic variation, which can be related to the experimental factors mentioned. For this position of test, OXPEKK presented the highest value of vertical displacement, followed by PEKK, PEEK, PMMA and Trilor.

In table 4.10, we can see that there is a pattern in the principal strains. PEEK has both the highest tensile and compressive strains, and PEKK has the lowest values.

Table 4.10: Average value of the principal strains obtained on VIC-3D software for the compression of the premolars in the framework (frontal view) with a 200N load.

Materials	**Load (N)**	ε_1 ($\mu\varepsilon$)	$\pm$ **sd** ($\mu\varepsilon$)	ε_2 ($\mu\varepsilon$)	$\pm$ **sd** ($\mu\varepsilon$)
PEEK		1441.9524	846.1330	-1226.9256	348.6031
PEKK		763.4989	159.8308	-576.4546	230.3073
PMMA	200	1127.4271	431.8363	-905.6927	399.0995
OXPEKK		1030.2979	173.3812	-806.5523	234.8480
Trilor		1126.4238	234.6404	-662.6103	251.7847

Compression of the premolars (lateral view)

These position of test aimed to obtain a closer view of the molars. The results of the machine are displayed in table 4.11 and figure 4.18. The values obtained in the software VIC-3D are presented in tables 4.12 and 4.13 and figure 4.19.

Table 4.11: Average displacement obtained on the Shimadzu machine for the compression of the premolars in the framework (lateral view).

Materials	Load (N)	Mean (mm)	± Standard Deviation (mm)
PEEK	100	0.6905	0.0220
	200	0.9594	0.0321
PEKK	100	0.6161	0.0059
	200	0.8761	0.0120
PMMA	100	0.5095	0.0911
	200	0.7831	0.1029
OXPEKK	100	0.7235	0.1168
	200	0.9864	0.1134
Trilor	100	0.7073	0.0527
	200	0.8971	0.0539

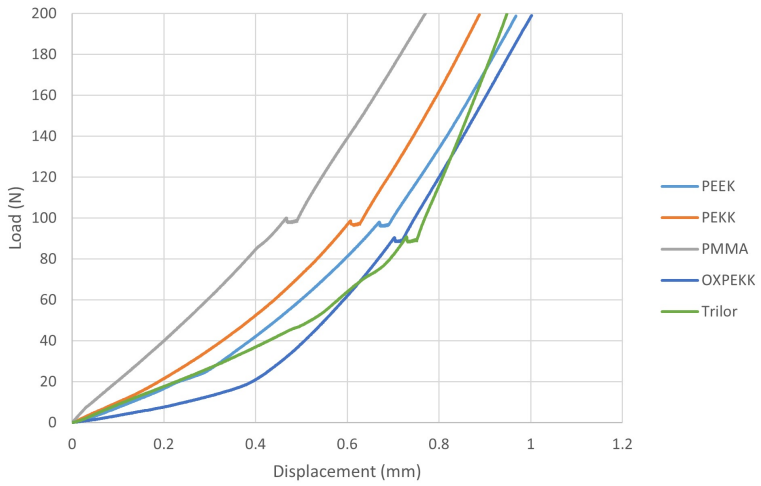

Figure 4.18: Vertical displacement of the load cell of the Shimadzu machine for the compression of the premolars in the framework (lateral view).

In the curves of figure 4.18 and as referred previously, the initial displacement close to zero was also removed because it was associated with small adjustments of the loading device in the initial phase of compression. However, some of the curves, namely OXPEKK and Trilor, still show high displacement at the beginning of loading. This behavior could be related to the flexibility of the testing material or the Technovit that supports the implants. Technovit has a modulus of elasticity

of about 2.2 GPa, which can mean that the initial displacement could be related to the compression of this material. OXPEKK and Trilor show the highest values of displacement for a 100N load compression, but for superior loads, the rate of displacement of Trilor drops significantly, which may indicate that the initial rate was influenced by other experimental factors. PMMA and PEKK present the lowest values of displacement, and PEEK and OXPEKK the highest.

Table 4.12: Average displacement obtained on the software VIC-3D for the compression of the premolars in the framework (lateral view).

Materials	**Load (N)**	**U (mm)**	**± sd (mm)**	**V (mm)**	**± sd (mm)**
PEEK	100	-0.2016	0.0135	0.0394	0.0286
	200	-0.3420	0.0186	0.0709	0.0399
PEKK	100	-0.1634	0.0053	0.0781	0.0127
	200	-0.2791	0.0033	0.1243	0.0156
PMMA	100	-0.0495	0.0115	-0.0109	0.0417
	200	-0.1186	0.0324	-0.0063	0.0487
OXPEKK	100	-0.2434	0.1088	0.0535	0.1220
	200	-0.3821	0.1154	0.0920	0.1211
Trilor	100	-0.2395	0.0768	0.2354	0.0560
	200	-0.3005	0.0888	0.2543	0.0656

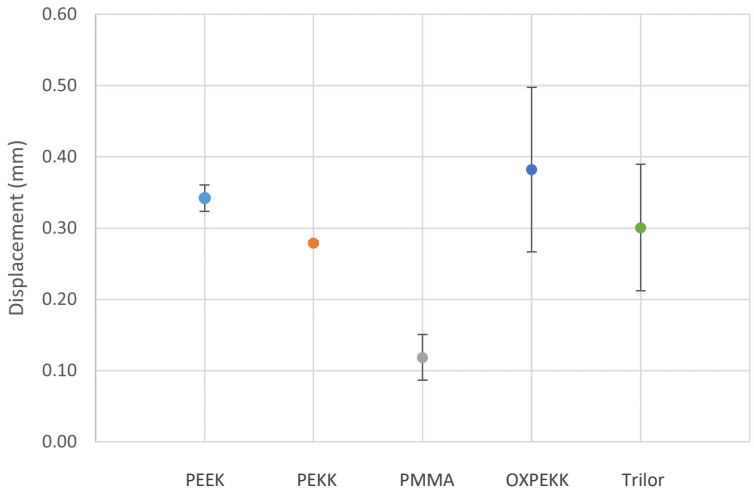

Figure 4.19: Absolute value of vertical displacement (U) in millimeters (mm) obtained on VIC-3D for the compression of the premolars in the framework (lateral view) under a 200N load. The bars in each point represent the standard deviation.

Once again, OXPEKK displays the highest mean value of displacement for the 200N load compression, followed by PEEK, Trilor, PEKK, and PMMA. Nonetheless, the difference is not that big since OXPEKK is the only polymer made by an AM technique.

The results of the principal strains (table 4.13) show significantly higher mean of positive deformation in Trilor with high value of standard deviation, which are not expected since it is the material with higher modulus of elasticity. OXPEKK also presents a high value of tensile strain. In terms of negative deformation, the higher values are noted in PEEK and PEKK.

Table 4.13: Average value of the principal strains obtained on VIC-3D software for the compression of the premolars in the framework (lateral view) with a 200N load.

Materials	**Load (N)**	ε_1 ($\mu\varepsilon$)	$\pm$ **sd** ($\mu\varepsilon$)	ε_2 ($\mu\varepsilon$)	$\pm$ **sd** ($\mu\varepsilon$)
PEEK		341.3391	100.8812	-1655.3645	686.8484
PEKK		149.5644	112.7286	-1076.3840	757.7239
PMMA	200	296.8488	44.0232	-219.1084	64.6470
OXPEKK		759.7628	208.6258	-789.9286	203.9994
Trilor		2869.2915	3337.2320	-938.0586	2650.6283

4.4 Experimental Study - Complete Prosthesis

In the complete prosthesis, the two types of AM techniques previously explained were tested. The only positions tested are depicted in figure 4.20, along with the selected regions of interest, represented by white rectangles.

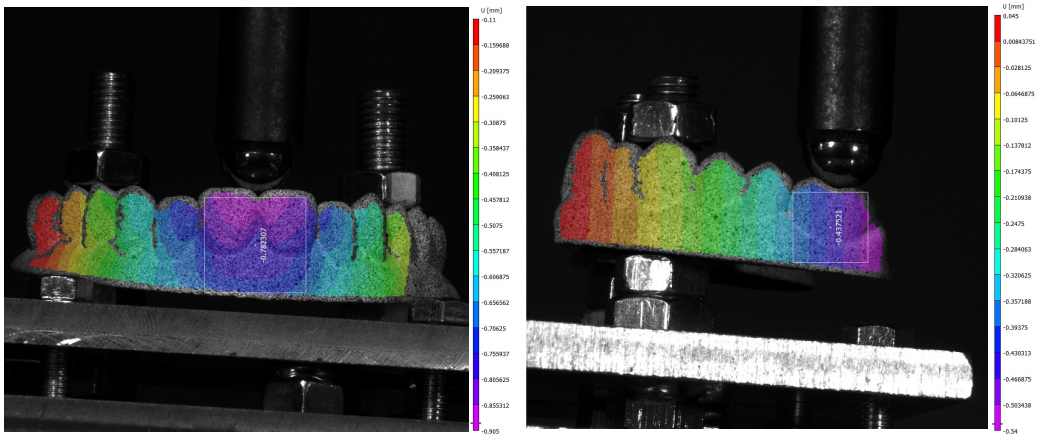

(a) **(b)**

Figure 4.20: Regions of interest represented by a white rectangle and selected in each position: (a) Incisors and (b) Molar. The two prosthesis of the photos are made of OXPEKK, and the photos were taken at a 200N load compression. The scales on the right of each picture are automatically generated and different in each position.

These prostheses were supported by M7 screws, as shown in the image. When tightening the screws, sometimes extra force was applied, which led to some unwanted fractures. A sample of OXPEKK was fractured and a new sample needed to be used (4.21).

(a) **(b)**

Figure 4.21: Fracture on the complete prosthesis of OXPEKK, signaled by the arrow.

Compression of the incisors

First, the results of the machine for the first position are displayed in table 4.14 and figure 4.22. Then, the values obtained in the software VIC-3D are presented in tables 4.15 and 4.16 and figure 4.23.

Table 4.14: Average displacement obtained on the Shimadzu machine for the compression of the incisors in the complete prosthesis.

Materials	Load (N)	Mean (mm)	± Standard Deviation (mm)
PEEK	100	0.2407	0.0030
	200	0.5049	0.0063
PEKK	100	0.3329	0.0354
	200	0.6741	0.0828
PMMA (milled)	100	0.4506	0.0575
	200	1.1237	0.0564
PMMA (printed)	100	1.2686	0.3325
	200	2.6428	0.7583
OXPEKK	100	0.4803	0.0240
	200	0.9999	0.0951
Trilor	100	0.3632	0.0033
	200	0.5846	0.0149
ABS	100	0.9549	0.0840
	200	1.8501	0.1521
HIPS	100	1.1380	0.0337
	200	2.1124	0.0037

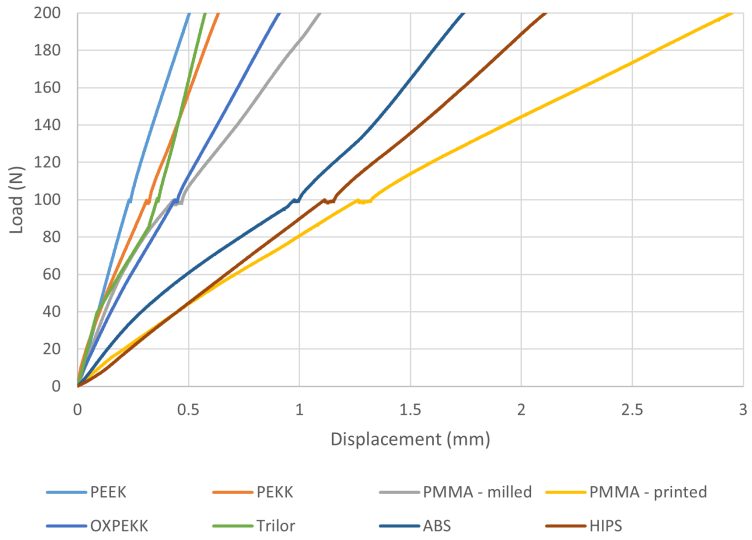

Figure 4.22: Vertical displacement of the load cell of the Shimadzu machine for the compression of the incisors in the complete prosthesis.

The differences between the polymers obtained with FDM and the other materials are clear, with the first ones presenting much bigger values of displacement in the load cell. Printed PMMA and HIPS show similar behavior for loads under 50N, but then the displacement rate of PMMA increases.

Table 4.15: Average displacement obtained on the software VIC-3D for the compression of the incisors in the complete prosthesis.

Materials	Load (N)	U (mm)	± sd (mm)	V (mm)	± sd (mm)
PEEK	100	-0.1465	0.0158	-0.0349	0.0087
	200	-0.3579	0.0038	-0.0119	0.0092
PEKK	100	-0.2143	0.0387	0.0175	0.0533
	200	-0.5107	0.0766	0.0171	0.0230
PMMA (milled)	100	-0.4014	0.1842	-0.0063	0.0101
	200	-0.9038	0.4132	-0.0542	0.0427
PMMA (printed)	100	-0.8661	0.0652	-0.0285	0.0585
	200	-1.8089	0.1710	-0.0508	0.0534
OXPEKK	100	-0.2835	0.0285	0.0133	0.0357
	200	-0.6886	0.0842	0.0567	0.0630
Trilor	100	-0.2846	0.0314	0.6336	0.7843
	200	-0.4892	0.0415	0.6574	0.7857
ABS	100	-0.7789	0.0450	0.0611	0.0156
	200	-1.5066	0.1209	0.1088	0.0147
HIPS	100	-0.6129	0.0263	0.0082	0.0026
	200	-1.4038	0.0234	0.0271	0.0030

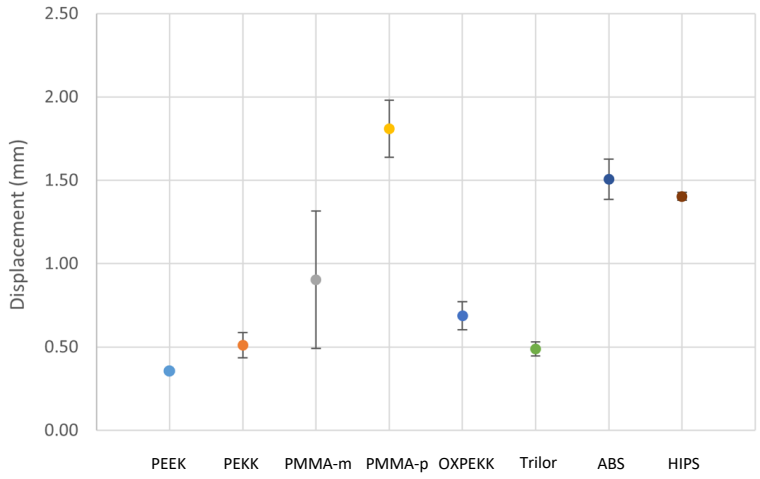

Figure 4.23: Absolute value of vertical displacement (U) in millimeters (mm) obtained on VIC-3D for the compression of the incisors in the complete prosthesis under a 200N load. The bars in each point represent the standard deviation.

The prosthesis made of PMMA broke in the last test but material continued to bear load, which may have to do with the ductility of the material (see figure 4.24).

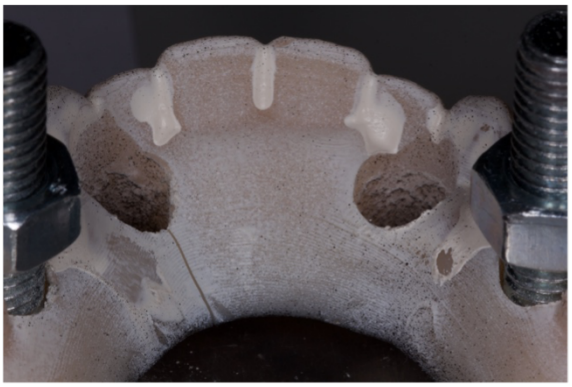

Figure 4.24: Fracture of the prosthesis made of PMMA.

The first thing to note is the decrease in the difference between the results of the machine and the software VIC, which makes them a lot more similar. It is also possible to confirm the higher values of displacement of the polymers obtained with FDM that stand out from the rest. OXPEKK maintains the behavior previously shown, closer to the milled polymers and Trilor.

The results obtained for the principal strains compiled in table 4.16 show higher values of positive and negative deformation in the FDM polymers. Milled PMMA and OXPEKK are the next highest values, followed by the other polymers and Trilor.

Table 4.16: Average value of the principal strains obtained on VIC-3D software for the compression of the incisors in the complete prosthesis with a 200N load.

Materials	**Load (N)**	ε_1 ($\mu\varepsilon$)	$\pm$ **sd** ($\mu\varepsilon$)	ε_2 ($\mu\varepsilon$)	$\pm$ **sd** ($\mu\varepsilon$)
PEEK		1227.5855	34.3711	-2039.2467	188.6838
PEKK		1555.9766	88.7423	-2218.3964	145.7651
PMMA (milled)		2059.1842	59.1323	-2403.4959	135.3185
PMMA (printed)	200	6144.7072	577.7299	-11293.1318	1026.1933
OXPEKK		1758.0426	36.2507	-2741.8558	13.8331
Trilor		449.8933	82.9283	-1060.0364	561.9287
ABS		3660.0560	141.4230	-6323.4109	444.8411
HIPS		6666.4112	121.7831	-10407.8207	97.9587

Compression of the molar

The results of the machine are displayed in table 4.17 and figure 4.26. The values obtained in the software VIC-3D are presented in tables 4.18, 4.19 and figure 4.27. For the compression of the molar, the prosthesis made of HIPS broke when the load reached a value of 140.252N. That is the reason for the absence of values of this material for the 200N load compression. The fracture is depicted in figure 4.25.

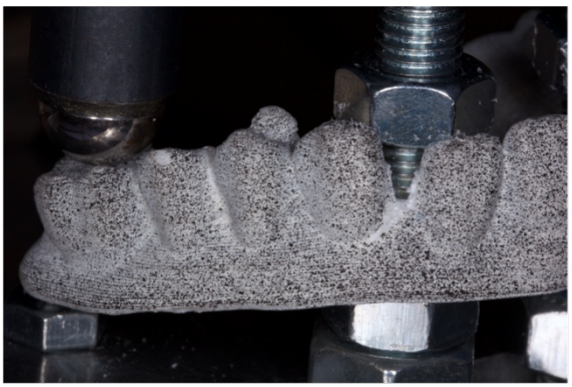

Figure 4.25: Fracture of the prosthesis made of HIPS.

Table 4.17: Average displacement obtained on the Shimadzu machine for the compression of the molar in the complete prosthesis.

Materials	Load (N)	Mean (mm)	± Standard Deviation (mm)
PEEK	100	0.5218	0.0921
	200	0.8791	0.0637
PEKK	100	0.2985	0.0187
	200	0.5479	0.0178
PMMA (milled)	100	0.4506	0.0575
	200	1.1237	0.0564
PMMA (printed)	100	1.9111	0.1325
	200	3.4210	0.0268
OXPEKK	100	0.7618	0.0160
	200	1.1474	0.0066
Trilor	100	0.3783	0.0995
	200	0.6245	0.1020
ABS	100	0.8010	0.1696
	200	1.3042	0.3600
HIPS	100	1.9565	-
	200	-	-

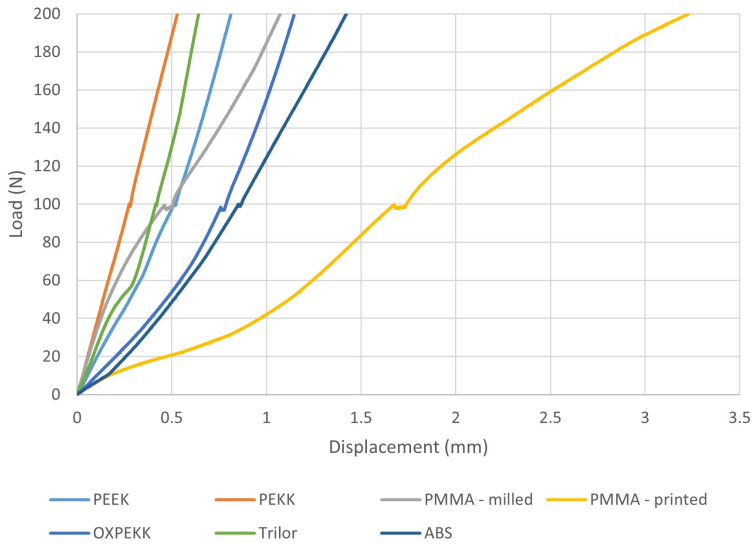

Figure 4.26: Vertical displacement of the load cell of the Shimadzu machine for the compression of the molar in the framework.

The behavior of the prosthesis when the molar is compressed is similar to that noted in the incisors. Printed PMMA still shows the highest values of displacement, followed by the other AM polymers, ABS and OXPEKK.

Table 4.18: Average displacement obtained on the software VIC-3D for the compression of the molar in the complete prosthesis.

Materials	Load (N)	U (mm)	± sd (mm)	V (mm)	± sd (mm)
PEEK	100	-0.3733	0.0449	0.0167	0.0365
	200	-0.6924	0.0336	0.0197	0.0284
PEKK	100	-0.2335	0.0616	0.0283	0.0444
	200	-0.4586	0.0834	0.0762	0.0424
PMMA (milled)	100	-0.6686	0.0222	0.1212	0.0176
	200	-1.3923	0.1594	0.0668	0.0314
PMMA (printed)	100	-1.7348	0.3067	-0.0450	0.0598
	200	-3.4123	0.3826	0.0621	0.0724
OXPEKK	100	-0.2105	0.0533	0.0211	0.0216
	200	-0.5187	0.0510	0.0859	0.0457
Trilor	100	-0.3067	0.0550	0.1063	0.0372
	200	-0.5047	0.0490	0.1968	0.0386
ABS	100	-0.5919	0.2057	-0.0147	0.0922
	200	-1.2157	0.2053	-0.0241	0.1288
HIPS	100	-1.6483	-	0.0938	-
	200	-	-	-	-

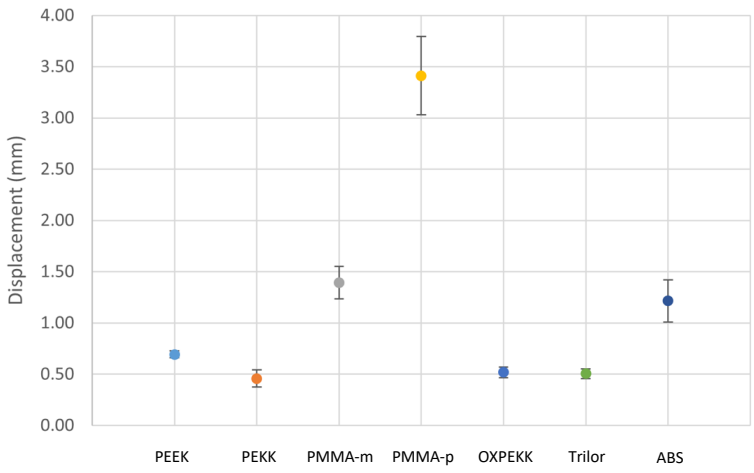

Figure 4.27: Absolute value of vertical displacement (U) in millimeters (mm) obtained on VIC-3D for the compression of the molar in the complete prosthesis under a 200N load. The bars in each point represent the standard deviation.

The results obtained in the software are the most similar to the ones obtained in the machine. The order of the materials from the highest to lowest displacement in the maximum load is: printed PMMA, milled PMMA, ABS, PEEK, OXPEKK, Trilor and PEKK.

The principal strains follow almost the same pattern as noted in the compression of the incisors. In table 4.19, we can see that the values of tensile strain are higher in the printed PMMA followed by HIPS. The same materials show higher compressive

strain. Curiously, OXPEKK show the lowest values for both the principal strains, which is a good indicator. The values presented for HIPS correspond to the last measurements before the structure broke.

Table 4.19: Average value of the principal strains obtained on VIC-3D software for the compression of the molar in the complete prosthesis with a 200N load.

Materials	**Load (N)**	ε_1 ($\mu\varepsilon$)	$\pm$ **sd** ($\mu\varepsilon$)	ε_2 ($\mu\varepsilon$)	$\pm$ **sd** ($\mu\varepsilon$)
PEEK		755.0788	173.6884	-1073.5217	457.2113
PEKK		496.0077	90.9196	-401.2316	156.9178
PMMA (milled)		736.0968	153.7857	-1820.2511	246.6229
PMMA (printed)	200	1301.4836	95.2510	-2634.0892	736.2366
OXPEKK		311.3866	78.8936	-387.4132	112.5792
Trilor		611.7565	156.9843	-735.4475	110.7535
ABS		773.8376	68.4243	-1187.7549	97.8938
HIPS		799.4960	-	-2121.6960	-

5

Conclusion and Future Work

The present work aimed to compare the performance of conventional non-polymeric frameworks with polymeric ones and test different types of fabrication, in order to understand if AM techniques are a viable option.

Metal, metal alloy, and fiber-reinforced composites were compared with polymers in the numeric study using two different models, loaded in the premolars. Model 1, the less realistic, revealed visible differences between the polymers and the rest of the materials but with similar critical regions. PMMA presented the highest values of displacement, then OXPEKK and PEEK, all reaching more than 2 μm. The same materials showed the lowest values of effective stress, in the same order.

Model 2, upgraded to be more realistic, was tested in the same way. These results confirmed the values obtained with Model 1, with a slight increase of the displacement values, reaching the value of 3 μm, and the effective stress.

In the experimental study, the emphasis was the comparison between structures made with SM and AM. Materials obtained with two different types of AM techniques were tested. Despite that, the analysis of the vertical displacement showed a pattern, with OXPEKK presenting higher values of displacement but with little difference from the other materials. It was expected that more rigid materials would present lower values of deformations for the same load, which doesn't always happen.

In the complete prostheses, polymers obtained by FDM showed way bigger values of displacement and deformations when compared to OXPEKK, fabricated by SLS. PEEK, PEKK, and Trilor presented the smallest values of displacement.

The two types of AM polymers fabricated show structural differences that influence their mechanical behavior. The inside of OXPEKK, obtained by SLS, is more compact than the polymers obtained by FDM, which have more visible printing lines that induce less compaction. The layers of the materials obtained by FDM are less unified, which causes higher displacement and deformation. OXPEKK also presents surface roughness that can be beneficial for the adhesion of prosthetic components.

Materials already tested in short follow-up studies such as PEEK, PEKK, and Trilor showed a favorable mechanical behavior, but other methods of fabrication need to be tested.

We can conclude that SLS is the better option of the two AM techniques studied and OXPEKK the best-tested material that meets the requirements of this study to replace conventional restorations: the lower modulus of elasticity, favorable structural and mechanical behavior and the fabrication by an AM technique. To confirm that this would be a good substitute material, a lot of further tests are necessary.

In terms of future work we can highlight different points, separating the numeric and experimental analysis.

In the numeric analysis:

- Increase the complexity of the models to better replicate the reality with the addition of more prosthetic parts and, if possible, biological components;
- Use different types of loads with new application sites and test new materials;
- Use more realistic material behavior, because it seems that some materials aren't linear elastic all the time as we assumed;
- Use time steps to apply load gradually.

In the experimental analysis:

- In accordance to what was previously said, the experiment can benefit from adding more components to the models, for example to simulate teeth and gingiva;
- The system to retain the models needs to be refined to prevent unwanted movements, mainly for the framework;
- Use strain gauges to measure strain in specific points of the models;
- Use tests of fatigue to repeatedly load the materials and try to determine the number of load cycles till failure of the different materials. This test would simulate the load cycles to which the prostheses are exposed in each meal, for example;
- Test an AM version of PEEK and PEKK, the high-performance polymers;
- Investigate new materials and AM techniques to fabricate them;
- Improve the quality of impression of polymers obtained in the laboratory with FDM and test the influence of different printing orientations;
- In high-performance polymers, highly inert, investigate the use of a primer or treatments to improve the superficial bioactivity of the materials without

changing the mechanical properties;

- Investigate and compare the performance of materials in degradation and enzymatic tests, that allow the simulation of some of the in vivo conditions. These tests take time and specific equipment, which can be a limitation.

For an even more realistic experiment, in vivo tests with AM fabricated frameworks or prostheses could be performed. First, as provisional restorations, showing the performance of the materials for 6 months, for example. Then as a permanent restoration for longer follow-ups.

Bibliography

[1] M. Kamath, "Changes in dentition across time and space: an evolutionary study of variations in size, shape and morphology of hominin and anatomically modern human premolars using geometric morphometrics (master dissertation)," *Faculty of Humanities of the University of Southampton*, 2015, Available on https://www.researchgate.net/publication/284859040.

[2] M. Atkinson, *Anatomy for Dental Students*. Oxford University Press, USA, 4 ed., 2013.

[3] E. Emami, R. F. De Souza, M. Kabawat, and J. S. Feine, "The impact of edentulism on oral and general health," *International Journal of Dentistry*, vol. 2013, 2013.

[4] N. Norton, *Netter's Head and Neck Anatomy for Dentistry*. Netter Basic Science, Elsevier, 3 ed., 2016.

[5] E. Furtado, "Complete line of implant." [Online], Available: = https://grabcad.com/library/complete-line-of-implant-1, [Accessed: 07-09-2021].

[6] Bioloren, "Trilor manual, the solution for a non-metal dentistry." [Online], Available: = https://dent-thel.com/wp-content/uploads/2019/06/TrilorDiscos.pdf, [Accessed: 10-09-2021].

[7] A. Passaretti, G. Petroni, G. Miracolo, V. Savoia, A. Perpetuini, and A. Cicconetti, "Metal free, full arch, fixed prosthesis for edentulous mandible rehabilitation on four implants," *Journal of Prosthodontic Research*, vol. 62, no. 2, pp. 264–267, 2018.

[8] A. Bhargav, V. Sanjairaj, V. Rosa, L. W. Feng, and J. Fuh YH, "Applications of additive manufacturing in dentistry: A review," *Journal of Biomedical Materials Research - Part B Applied Biomaterials*, vol. 106, no. 5, pp. 2058–2064, 2018.

[9] M. Revilla-León and M. Özcan, "Additive Manufacturing Technologies Used for Processing Polymers: Current Status and Potential Application in Prosthetic Dentistry," *Journal of Prosthodontics*, vol. 28, no. 2, pp. 146–158, 2019.

[10] E. Palermo, "What is selective laser sintering?." [Online], Available: = https://www.livescience.com/38862-selective-laser-sintering.html, [Accessed: 20-09-2021].

[11] S. Najeeb, M. S. Zafar, Z. Khurshid, and F. Siddiqui, "Applications of polyetheretherketone (PEEK) in oral implantology and prosthodontics," *Journal of Prosthodontic Research*, vol. 60, no. 1, pp. 12–19, 2016.

[12] Arkema, "The kepstan pekk brochure)." [Online], Available: = https://www.extrememate rials-arkema.com/en/product-families/kepstan-pekk-polymer-range/?$_g a$ = 2.127005448.40392425.1632249579 − 1773881191.1632249579, [*Accessed* : 20 − 09 − 2021].

[13] S. Aldrich, "Poly(methyl methacrylate)." [Online], Available: = https://www.sigmaaldrich.com/PT/en/substance/polymethylmethacrylate123459011147, [Accessed: 20-09-2021].

[14] C. Mariano Domingues da Silva, A. L. A. Silva, R. Pacheco, and A. M. Rocco, "Conductivity and Thermal Behaviour of Sulfonated ABS Membranes for Fuel Cell Applications," *ECS Transactions*, vol. 25, no. 1, pp. 881–889, 2019.

[15] P. S. L. Center, "Polystyrene." [Online], Available: = https://www.pslc.ws/macrog/styrene.htm, [Accessed: 20-09-2021].

[16] J. H. Oh, X. An, S. M. Jeong, and B. H. Choi, "A digital technique for fabricating an interim implant-supported fixed prosthesis immediately after implant placement in patients with complete edentulism," *Journal of Prosthetic Dentistry*, vol. 121, no. 1, pp. 26–31, 2019.

[17] D. L. Logan, *A first course in the finite element method*, vol. 3. Thomson, 1987.

[18] Z.-Z. Tang, "Three-dimensional digital image correlation system for deformation measurement in experimental mechanics," *Optical Engineering*, vol. 49, no. 10, p. 103601, 2010.

[19] D. Sirandoni, E. Leal, B. Weber, P. Noritomi, R. Fuentes, and E. Borie, "Effect of Different Framework Materials in Implant-Supported Fixed Mandibular Prostheses: A Finite Element Analysis," *The International Journal of Oral Maxillofacial Implants*, vol. 34, no. 6, pp. e107–e114, 2019.

[20] K.-S. Lee, S.-W. Shin, S.-P. Lee, J.-E. Kim, J.-H. Kim, and J.-Y. Lee, "Comparative Evaluation of a Four-Implant–Supported Polyetherketoneketone Framework Prosthesis: A Three-Dimensional Finite Element Analysis Based on Cone Beam Computed Tomography and Computer-Aided Design," *The International Journal of Prosthodontics*, vol. 30, no. 6, pp. 581–585, 2017.

[21] A. Maandi, J. Porteus, and B. Roberts, "OsteoFab ® Technology," *OPM*, pp. 1–5, 2020.

[22] E. Komurlu, F. Cihangir, A. Kesimal, and S. Demir, "Effect of Adhesive Type on the Measurement of Modulus of Elasticity Using Electrical Resistance Strain Gauges," *Arabian Journal for Science and Engineering*, vol. 41, no. 2, pp. 433–441, 2016.

[23] G. Spagnuolo and R. Sorrentino, "The Role of Digital Devices in Dentistry: Clinical Trends and Scientific Evidences," *Journal of Clinical Medicine*, vol. 9, no. 6, p. 1692, 2020.

[24] J. Legaz, D. Karasan, V. Fehmer, and I. Sailer, "The 3D-printed prototype: a new protocol for the evaluation and potential adaptation of monolithic all-ceramic restorations before finalization," *Quintessence International*, vol. 51, no. 7, pp. 538–544, 2020.

[25] I. Papathanasiou, P. Kamposiora, G. Papavasiliou, and M. Ferrari, "The use of PEEK in digital prosthodontics: A narrative review," *BMC Oral Health*, vol. 20, no. 1, pp. 1–11, 2020.

[26] P. E. Petersen, "The World Oral Health Report 2003: Continuous improvement of oral health in the 21st century - The approach of the WHO Global Oral Health Programme," *Community Dentistry and Oral Epidemiology*, vol. 31, no. SUPPL. 1, pp. 3–24, 2003.

[27] A. G. Payne, N. H. Alsabeeha, M. A. Atieh, M. Esposito, S. Ma, and M. Anas El-Wegoud, "Interventions for replacing missing teeth: Attachment systems for implant overdentures in edentulous jaws," *Cochrane Database of Systematic Reviews*, vol. 2018, no. 10, 2018.

[28] J. F. Stephen F. Rosenstiel, Martin F. Land, *Contemporary Fixed Prosthodontics*. Elsevier, 5 ed., 2016.

[29] R. Luthra and P. Pathania, "Rehabilitation With Implant Supported Fixed Prosthesis- A Case Report," *European Journal of Experimental Biology*, vol. 08, no. 01, 2018.

[30] K. Chochlidakis, E. Einarsdottir, A. Tsigarida, P. Papaspyridakos, D. Romeo, A. B. Barmak, and C. Ercoli, "Survival rates and prosthetic complications of implant fixed complete dental prostheses: An up to 5-year retrospective study," *Journal of Prosthetic Dentistry*, vol. 124, no. 5, pp. 539–546, 2020.

[31] A. Messias, M. A. Neto, A. M. Amaro, V. M. Lopes, and P. Nicolau, "Mechanical evaluation of implant-assisted removable partial dentures in kennedy class i patients: Finite element design considerations," *Applied Sciences (Switzerland)*, vol. 11, no. 2, pp. 1–18, 2021.

[32] T. F. Alghazzawi, "Advancements in CAD/CAM technology: Options for practical implementation," *Journal of Prosthodontic Research*, vol. 60, no. 2, pp. 72–84, 2016.

[33] M. Revilla-León, M. J. Meyers, A. Zandinejad, and M. Özcan, "A review on chemical composition, mechanical properties, and manufacturing work flow of additively manufactured current polymers for interim dental restorations," *Journal of Esthetic and Restorative Dentistry*, vol. 31, no. 1, pp. 51–57, 2019.

[34] C. West and X. Wang, "Modeling of selective laser sintering/selective laser melting," *Laser 3D Manufacturing IV*, vol. 10095, p. 1009506, 2017.

[35] A. Tahayeri, M. C. Morgan, A. P. Fugolin, D. Bompolaki, A. Athirasala, C. S. Pfeifer, J. L. Ferracane, and L. E. Bertassoni, "3D printed versus conventionally cured provisional crown and bridge dental materials," *Dental Materials*, vol. 34, no. 2, pp. 192–200, 2018.

[36] S. Y. Bae, J. Y. Park, I. D. Jeong, H. Y. Kim, J. H. Kim, and W. C. Kim, "Three-dimensional analysis of marginal and internal fit of copings fabricated with polyetherketoneketone (PEKK) and zirconia," *Journal of Prosthodontic Research*, vol. 61, no. 2, pp. 106–112, 2017.

[37] H. Alqurashi, Z. Khurshid, A. U. Y. Syed, S. Rashid Habib, D. Rokaya, and M. S. Zafar, "Polyetherketoneketone (PEKK): An emerging biomaterial for oral implants and dental prostheses," *Journal of Advanced Research*, vol. 28, pp. 87–95, 2021.

[38] U. Ali, K. J. B. A. Karim, and N. A. Buang, "A Review of the Properties and Applications of Poly (Methyl Methacrylate) (PMMA)," *Polymer Reviews*, vol. 55, no. 4, pp. 678–705, 2015.

[39] P. Proussaefs, "Use of a CAD-CAM poly(methyl methacrylate) interim pros-

thesis for direct intraoral splinting," *Journal of Prosthetic Dentistry*, vol. 118, no. 6, pp. 706–711, 2017.

[40] G. C. Gumbau and C. G. Oliag, "All-on-4 with tapered neck implants and a hybrid prosthesis with a fiberglass- reinforced structure," *Journal of Oral Science Rehabilitation*, vol. 5, no. 3, pp. 16–23, 2019.

[41] F. S. Kamelian, E. Saljoughi, P. Shojaee Nasirabadi, and S. M. Mousavi, "Modifications and research potentials of acrylonitrile/butadiene/styrene (ABS) membranes: A review," *Polymer Composites*, vol. 39, no. 8, pp. 2835–2846, 2018.

[42] F. Soriano-Corral, G. Morales, P. Acuña, E. Díaz-Barriga, B. Arellano, C. Vargas, and O. De La Paz, "Synthesis and characterization of high impact polystyrene from a heterogeneous styrene-rubber-polystyrene solution: Influence of PS concentration on the phase inversion, morphology and impact strength," *Macromolecular Symposia*, vol. 325-326, no. 1, pp. 177–183, 2013.

[43] A. Zulfi, A. Fauzi, D. Edikresnha, M. M. Munir, and Khairurrijal, "Synthesis of High-Impact Polystyrene Fibers using Electrospinning," *IOP Conference Series: Materials Science and Engineering*, vol. 202, no. 1, 2017.

[44] P. Maló, M. de Araújo Nobre, C. Moura Guedes, R. Almeida, A. Silva, N. Sereno, and J. Legatheaux, "Short-term report of an ongoing prospective cohort study evaluating the outcome of full-arch implant-supported fixed hybrid polyetheretherketone-acrylic resin prostheses and the All-on-Four concept," *Clinical Implant Dentistry and Related Research*, vol. 20, no. 5, pp. 692–702, 2018.

[45] J. H. Dawson, B. Hyde, M. Hurst, B. T. Harris, and W. S. Lin, "Polyetherketoneketone (PEKK), a framework material for complete fixed and removable dental prostheses: A clinical report," *Journal of Prosthetic Dentistry*, vol. 119, no. 6, pp. 867–872, 2018.

[46] K. C. Oh, J. H. Park, J. hee Lee, and H. S. Moon, "Treatment of a mandibular discontinuity defect by using a fibula free flap and an implant-supported fixed complete denture fabricated with a PEKK framework: A clinical report," *Journal of Prosthetic Dentistry*, vol. 119, no. 6, pp. 1021–1024, 2018.

[47] B. Wah, "Finite Element Method," *Wiley Encyclopedia of Computer Science and Engineering*, pp. 1–12, 2008.

[48] M. A. Neto, A. Amaro, R. Luis, J. Cirne, and R. Leal, *Engineering computation of structures: The finite element method*. Springer, 2015.

[49] S. Trivedi, "Finite element analysis: A boon to dentistry," *Journal of Oral Biology and Craniofacial Research*, vol. 4, no. 3, pp. 200–203, 2014.

[50] A. L. de Pereira Neves Messias, "Rehabilitation of kennedy class i patients with removable partial dentures: Retrospective clinical study and biomechanical analysis of implant-assisted options (doctoral dissertation)," *Faculty of Medicine of the University of Coimbra*, 2018, Available on http://hdl.handle.net/10316/87457.

[51] M. B. Ferreira, V. A. Barão, J. A. Delben, L. P. Faverani, A. C. Hipólito, and W. G. Assunção, "Non-linear 3D finite element analysis of full-arch implant-supported fixed dentures," *Materials Science and Engineering C*, vol. 38, no. 1, pp. 306–314, 2014.

[52] R. Tiossi, M. A. Vasco, L. Lin, H. J. Conrad, O. L. Bezzon, R. F. Ribeiro, and A. S. Fok, "Validation of finite element models for strain analysis of implant-supported prostheses using digital image correlation," *Dental Materials*, vol. 29, no. 7, pp. 788–796, 2013.

[53] R. F. Peixoto, B. S. H. Tonin, J. Martinelli, A. P. Macedo, and M. d. G. C. de Mattos, "In vitro digital image correlation analysis of the strain transferred by screw-retained fixed partial dentures supported by short and conventional implants," *Journal of the Mechanical Behavior of Biomedical Materials*, vol. 103, no. July 2019, 2020.

[54] K. GmbH, "Resins for materialography," *Kulzer GmbH - Product information*, 2017.

Appendices

A

Numerical Analysis - Links

A.1 Model 1

Table A.1: Mean, standard deviation and extreme values of displacement magnitude for the links of Model 1.

Materials	**Mean ± sd (μm)**	**Maximum (μm)**	**Minimum (μm)**	**ANOVA test**
PEEK	0.685 ± 1.102	5.835	0	
PEKK	0.627 ± 0.930	5.323	0	
PMMA	0.772 ± 1.149	6.600	0	
OXPEKK	0.713 ± 1.059	6.081	0	F(6,559384)=10025.9646,
Trilor	0.298 ± 0.434	2.431	0	p<0.001
Titanium	0.143 ± 0.205	1.137	0	
Co-Cr	0.101 ± 0.143	0.793	0	

Table A.2: Mean, standard deviation and extreme values of effective stress for the links of Model 1.

Materials	**Mean ± sd (MPa)**	**Maximum (MPa)**	**Minimum (MPa)**	**ANOVA test**
PEEK	4.840 ± 5.702	44.032	0.005	
PEKK	4.485 ± 5.280	40.910	0.008	
PMMA	5.376 ± 6.348	48.608	0.004	
OXPEKK	5.012 ± 5.906	45.491	0.004	F(6,559384)=12123.0364,
Trilor	2.471 ± 2.879	23.980	0.007	p<0.001
Titanium	1.444 ± 1.721	16.913	0.010	
Co-Cr	1.155 ± 1.389	14.938	0.005	

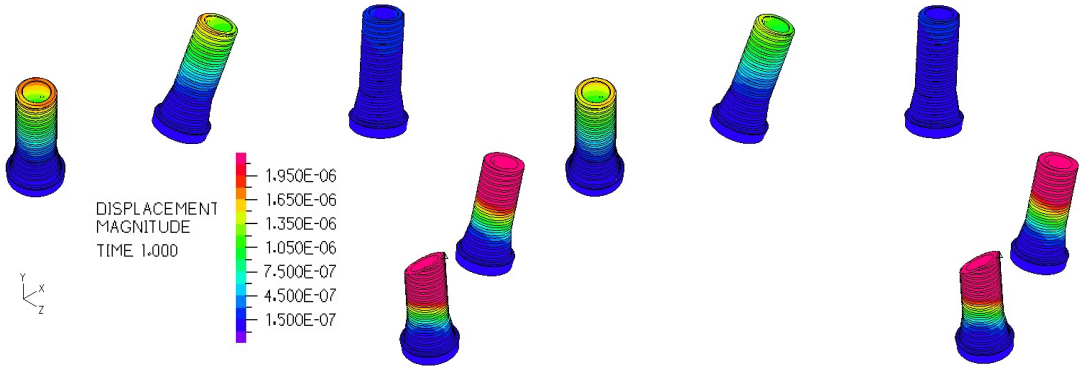

(a) PEEK

(b) PEKK

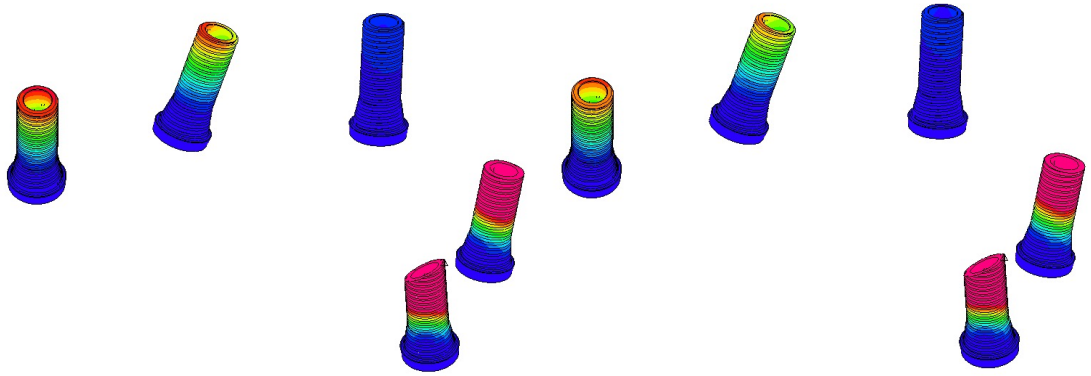

(c) PMMA

(d) OXPEKK

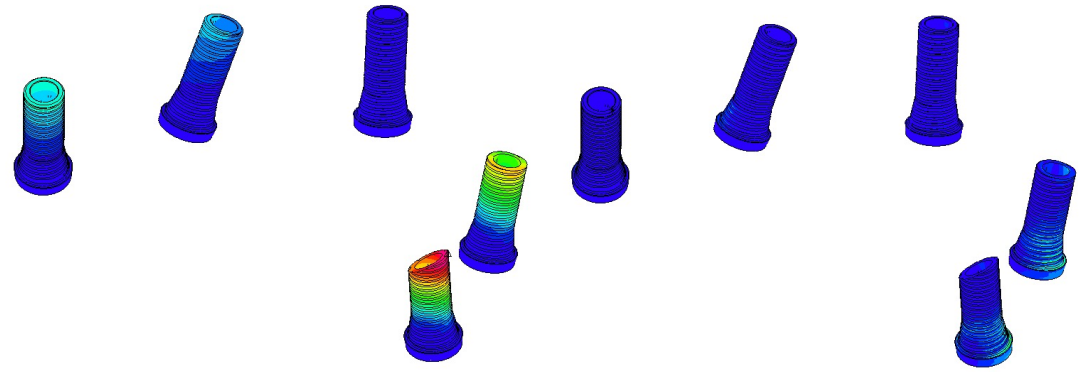

(e) Trilor

(f) Titanium

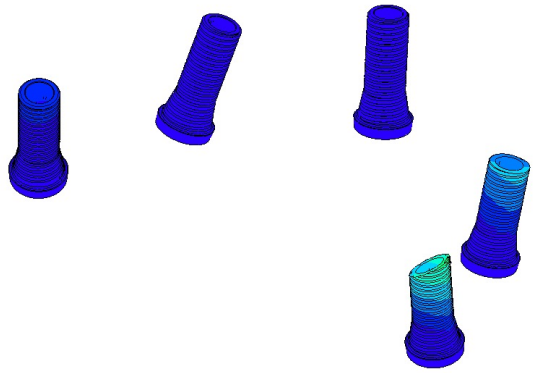

(g) Co-Cr

Figure A.1: Displacement magnitude of the links of Model 1.

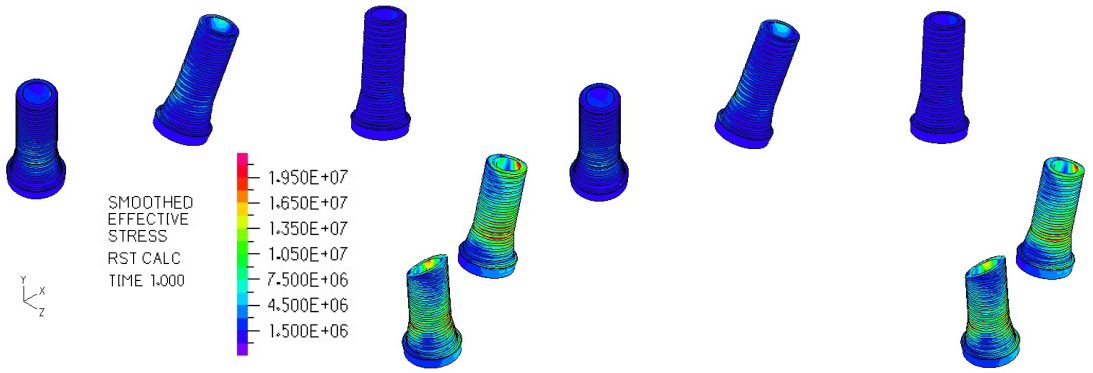

(a) PEEK

(b) PEKK

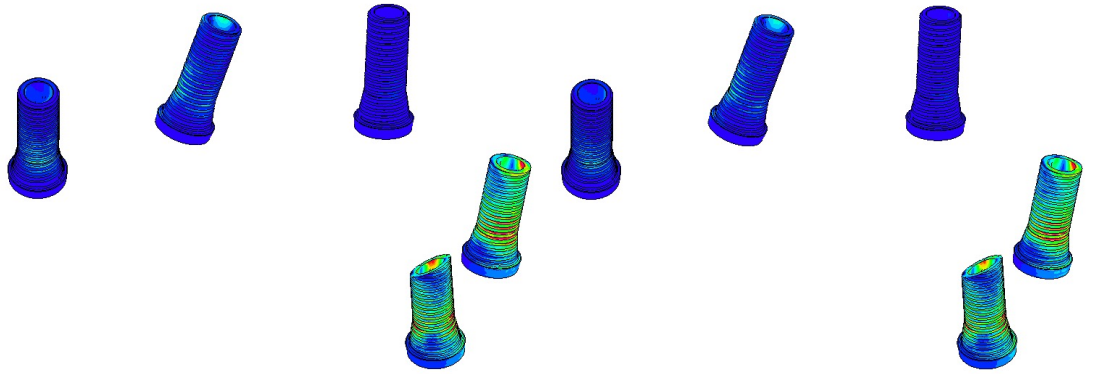

(c) PMMA

(d) OXPEKK

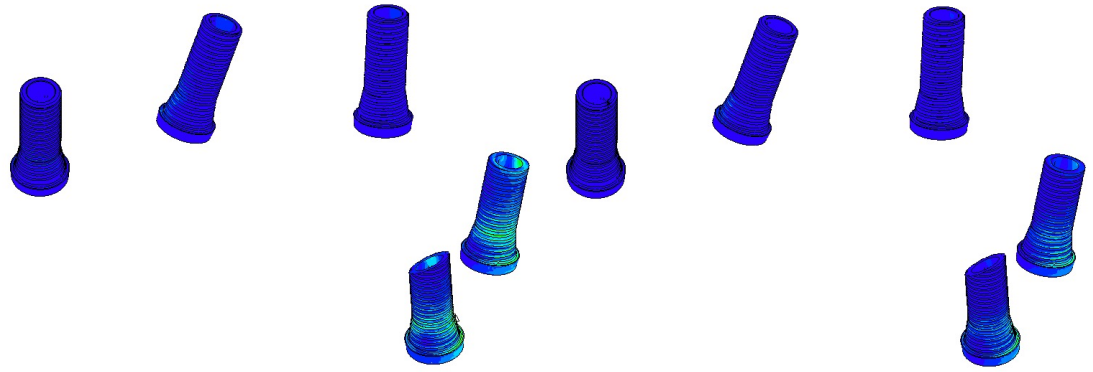

(e) Trilor

(f) Titanium

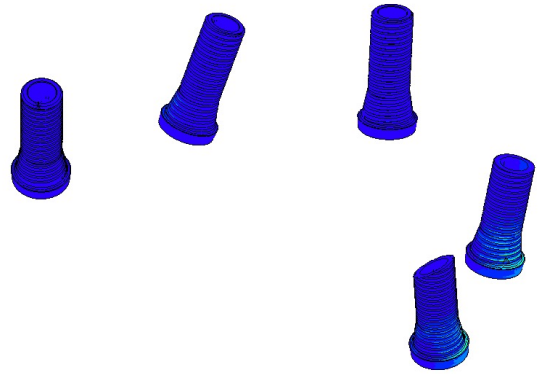

(g) Co-Cr

Figure A.2: Effective stress of the links of Model 1.

A.2 Model 2

Table A.3: Mean, standard deviation and extreme values of displacement magnitude for the links of Model 2.

Materials	**Mean ± sd (μm)**	**Maximum (μm)**	**Minimum (μm)**	**ANOVA test**
PEEK	1.107 ± 1.450	8.204	0.011	
PEKK	1.030 ± 1.343	7.585	0.014	
PMMA	1.222 ± 1.612	9.119	0.009	
OXPEKK	1.144 ± 1.502	8.500	0.010	F(6,559384)=11668.5221,
Trilor	0.546 ± 0.687	3.823	0.012	p<0.001
Titanium	0.264 ± 0.319	1.757	0.009	
Co-Cr	0.184 ± 0.213	1.173	0.014	

Table A.4: Mean, standard deviation and extreme values of effective stress for the links of Model 2.

Materials	**Mean ± sd (MPa)**	**Maximum (MPa)**	**Minimum (MPa)**	**ANOVA test**
PEEK	5.366 ± 5.590	43.384	0.047	
PEKK	4.964 ± 5.173	39.804	0.061	
PMMA	5.923 ± 6.224	48.616	0.027	
OXPEKK	5.560 ± 5.792	45.063	0.032	F(6,559384)=16862.9309,
Trilor	2.632 ± 2.771	26.599	0.031	p<0.001
Titanium	1.432 ± 1.582	18.010	0.010	
Co-Cr	1.129 ± 1.267	15.275	0.007	

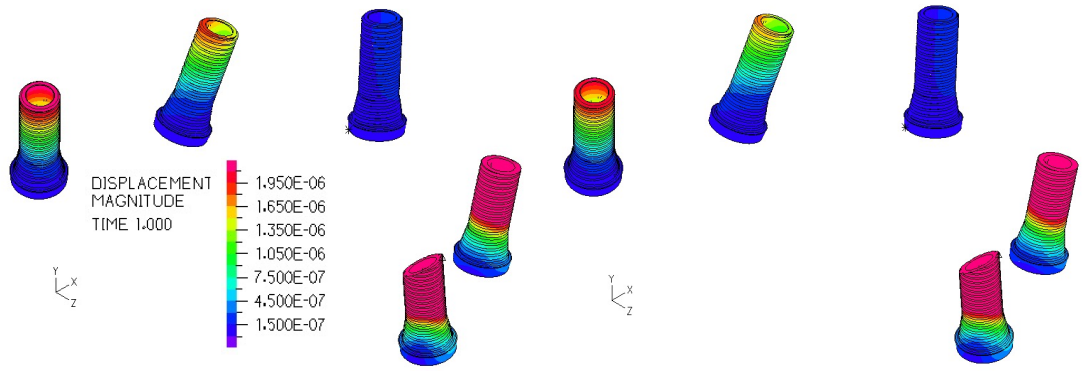

(a) PEEK

(b) PEKK

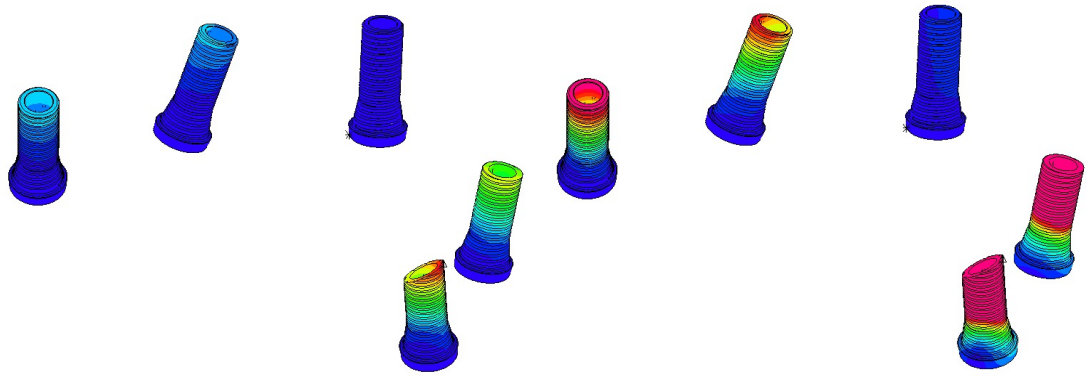

(c) PMMA

(d) OXPEKK

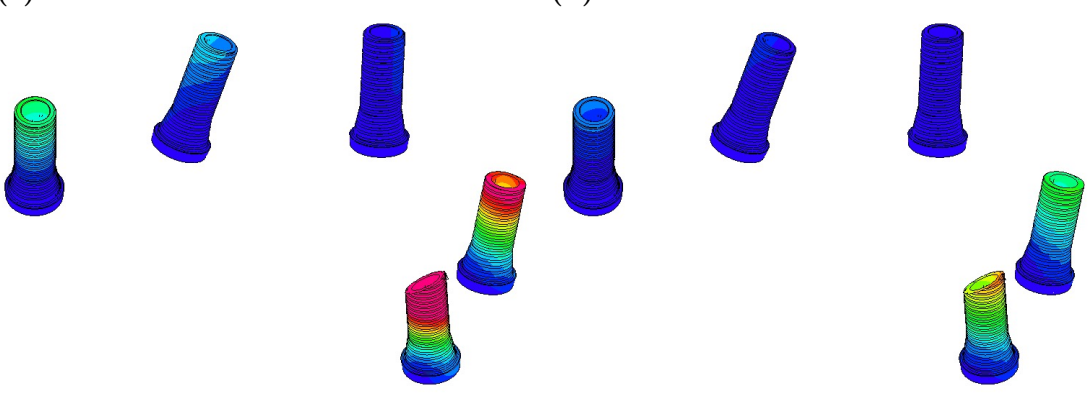

(e) Trilor

(f) Titanium

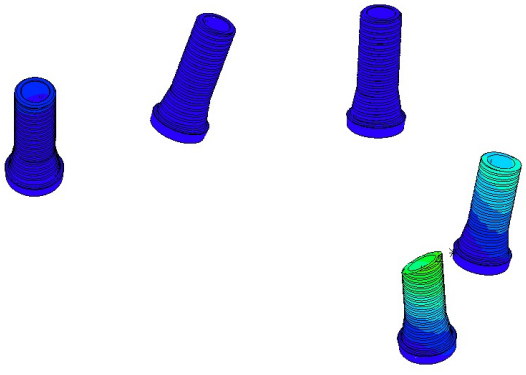

(g) Co-Cr

Figure A.3: Displacement magnitude of the links of Model 2.

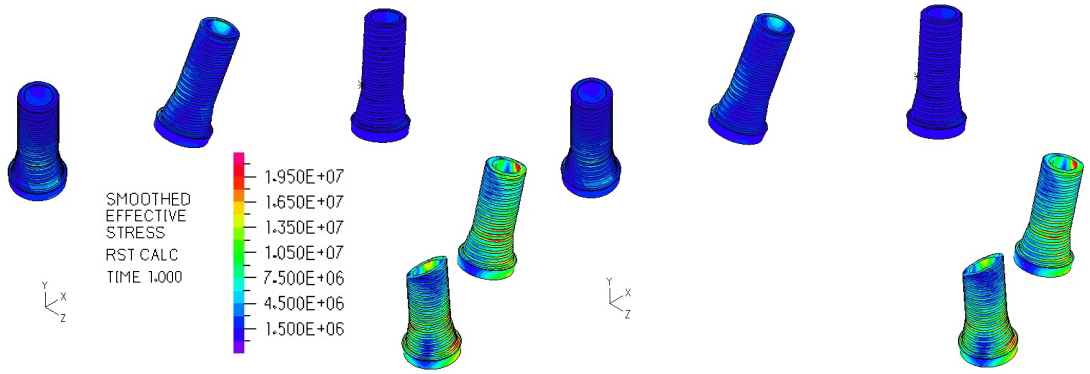

(a) PEEK

(b) PEKK

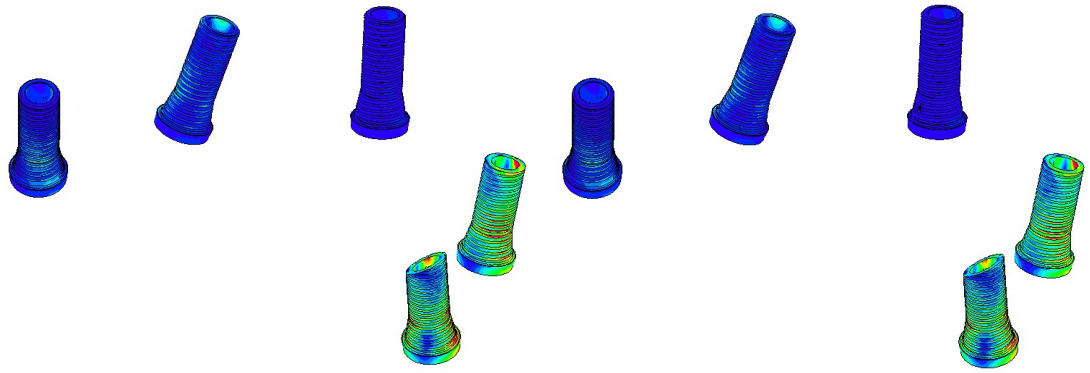

(c) PMMA

(d) OXPEKK

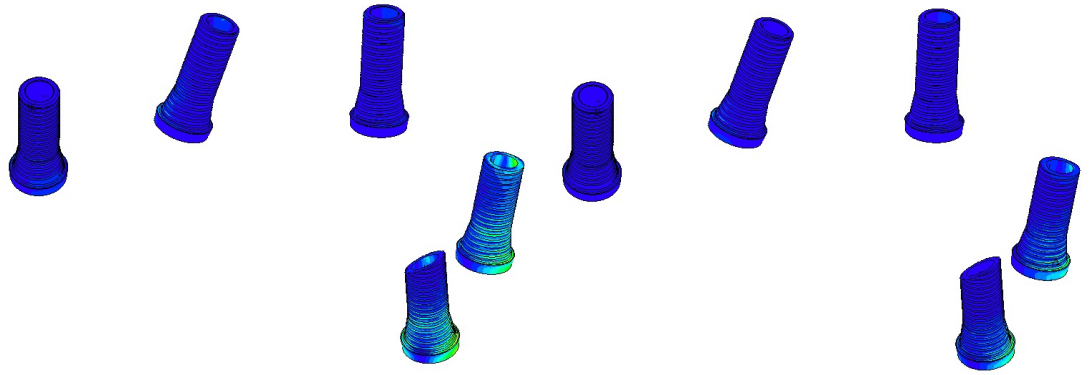

(e) Trilor

(f) Titanium

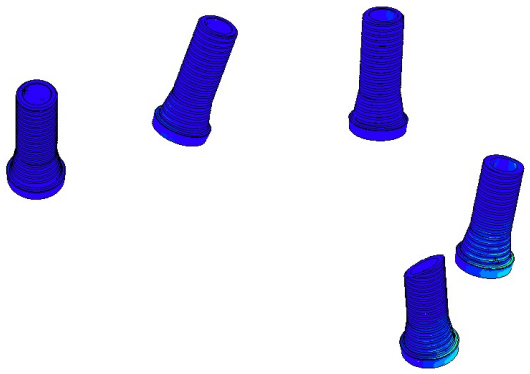

(g) Co-Cr

Figure A.4: Effective stress of Model 2.

A.3 Comparison between the models

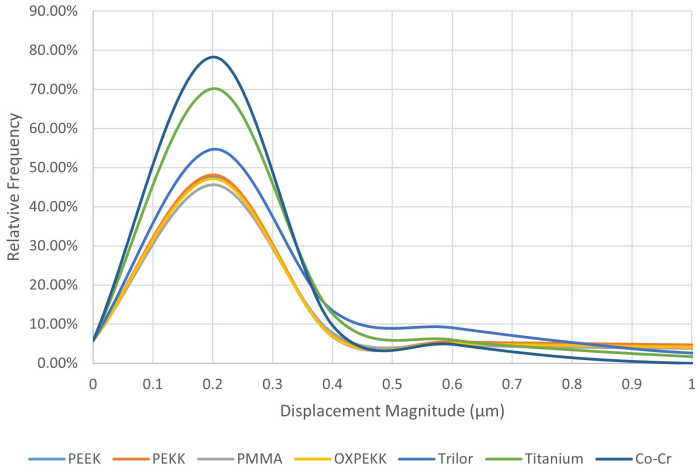

Figure A.5: Distribution of displacement magnitude values for the links of Model 1.

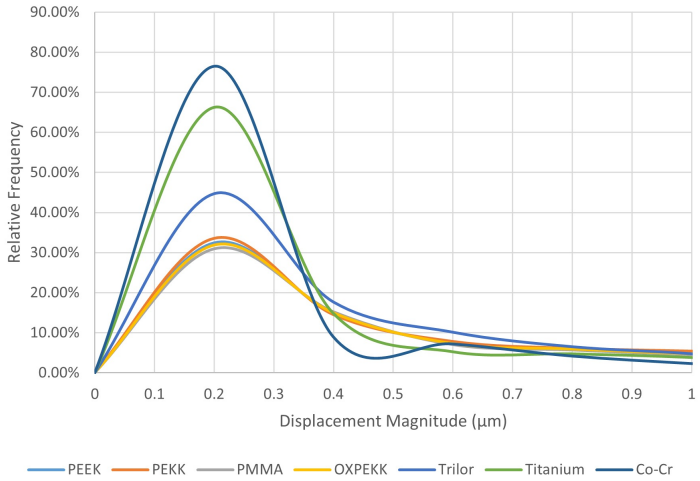

Figure A.6: Distribution of displacement magnitude values for the links of Model 2.

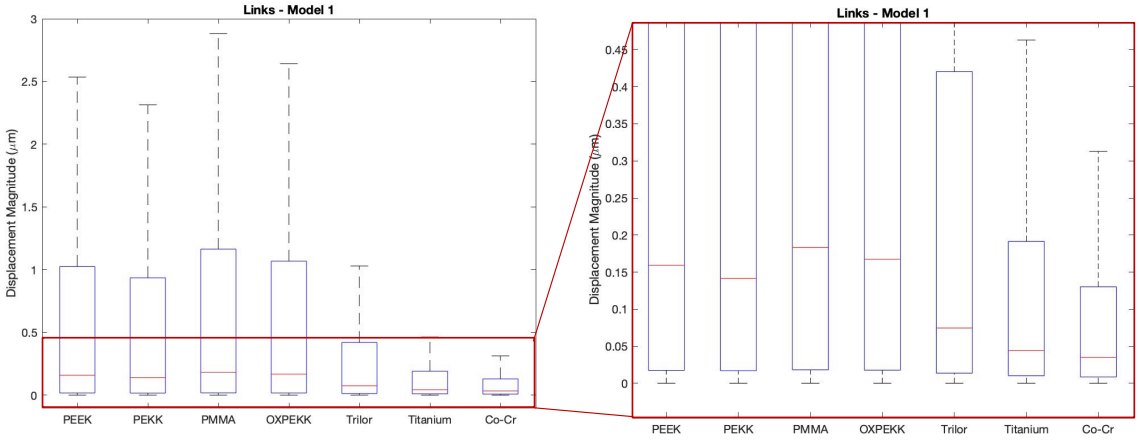

Figure A.7: Boxplot of the displacement magnitude in the links of Model 1. On the right, an approximation.

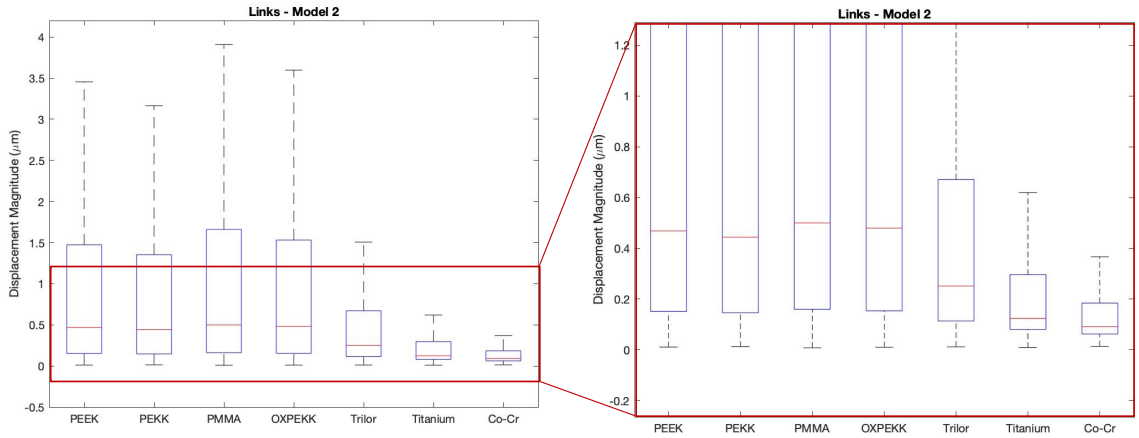

Figure A.8: Boxplot of the displacement magnitude in the links of Model 2. On the right, an approximation.

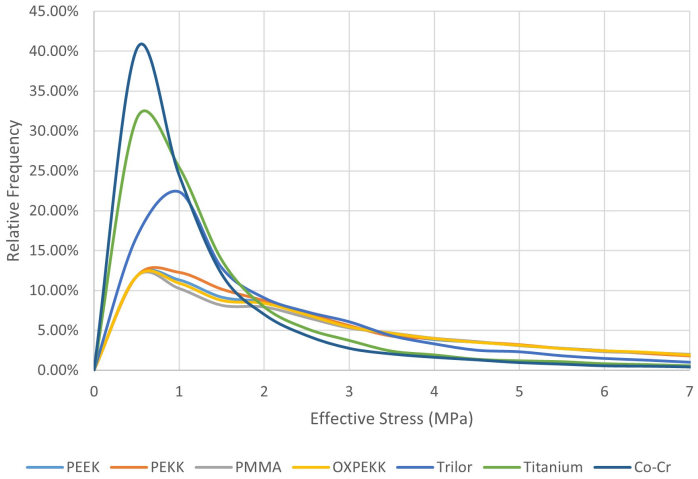

Figure A.9: Distribution of effective stress values for the links of Model 1.

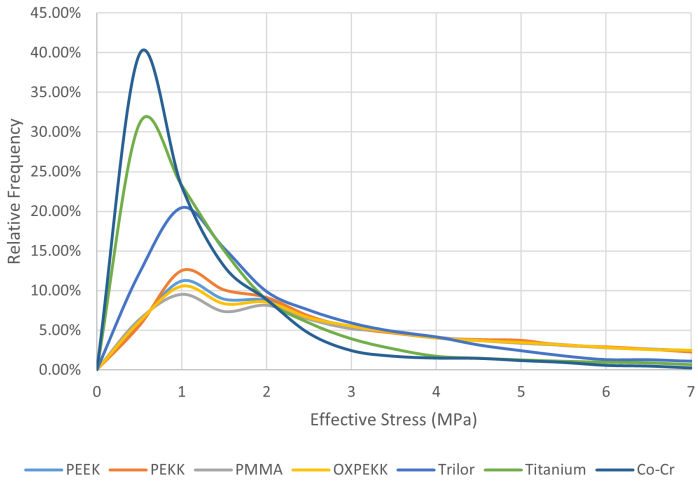

Figure A.10: Distribution of effective stress values for the links of Model 2.

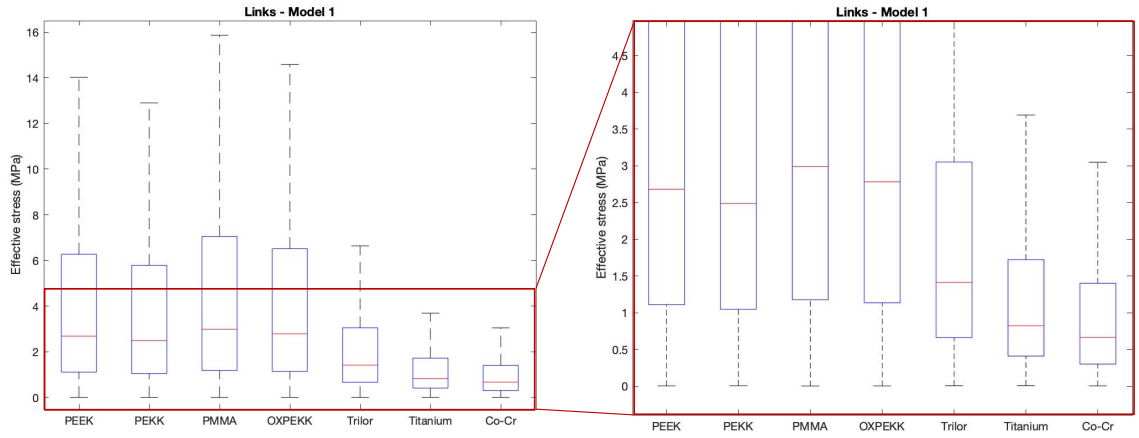

Figure A.11: Boxplot of the effective stress in the links of Model 1. On the right, an approximation.

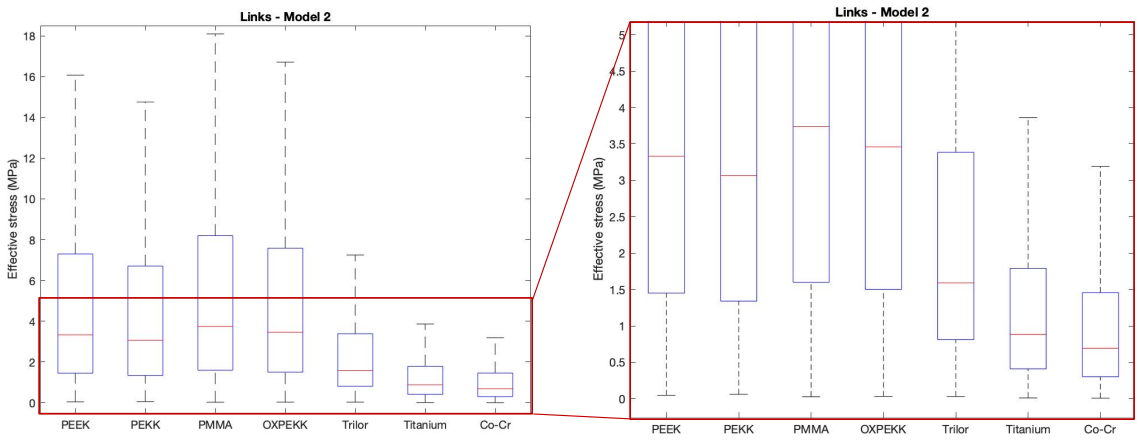

Figure A.12: Boxplot of the effective stress in the links of Model 2. On the right, an approximation.